Numerical investigation of nanofluids forced convection in circular tubes

V. Bianco, F. Chiacchio, O. Manca, S. Nardini

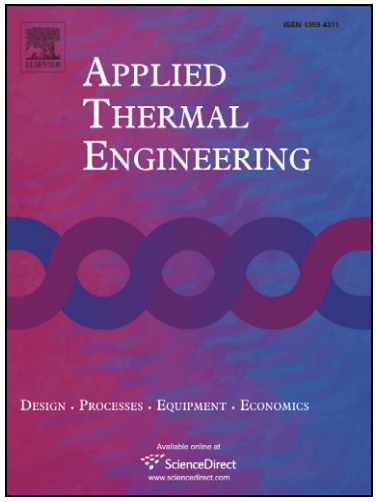

Numerical investigation of nanofluids forced convection in circular tubes

V. Bianco, F. Chiacchio, O. Manca, S. Nardini

PII: S1359-4311(09)00196-3
DOI: 10.1016/j.applthermaleng.2009.06.019
Reference: ATE 2845

To appear in: *Applied Thermal Engineering*

Received Date: 16 October 2008
Revised Date: 5 May 2009
Accepted Date: 19 June 2009

Please cite this article as: V. Bianco, F. Chiacchio, O. Manca, S. Nardini, Numerical investigation of nanofluids forced convection in circular tubes, *Applied Thermal Engineering* (2009), doi: 10.1016/j.applthermaleng.2009.06.019

NUMERICAL INVESTIGATION OF NANOFLUIDS FORCED CONVECTION IN CIRCULAR TUBES

V. Bianco, F. Chiacchio, O. Manca*, S. Nardini

Dipartimento di Ingegneria Aerospaziale e Meccanica

Seconda Università degli Studi di Napoli,

Via Roma 29, 81031 Aversa (CE) - ITALY

ABSTRACT

In this paper, developing laminar forced convection flow of a water–Al_2O_3 nanofluid in a circular tube, submitted to a constant and uniform heat flux at the wall, is numerically investigated.

A single and two-phase model (discrete particles model) is employed with either constant or temperature-dependent properties. The investigation is accomplished for size particles equal to 100 nm. The maximum difference in the average heat transfer coefficient between single and two phase models results is about 11%.

Convective heat transfer coefficient for nanofluids is greater than that of the base liquid. Heat transfer enhancement increases with the particle volume concentration, but it is accompanied by increasing wall shear stress values. Higher heat transfer coefficients and lower shear stresses are detected in the case of temperature dependents models. The heat transfer always improves, as Reynolds number increases, but it is accompanied by an increase of shear stress too.

Moreover a comparison with data present in the literature is carried out.

Keywords: Nanofluids; Nanoparticles; Discrete phase model; Laminar convection

*Corresponding author. Tel.: +39 081 5010 217; fax: +39 081 5010 204
E-mail address: oronzio.manca@unina2.it (O. Manca)

NOMENCLATURE

Cp	Specific heat of the fluid, J/kgK
D	Tube diameter, m
d	Particles diameter, m
δV	Cell volume, m^3
g	Gravitational acceleration, m/s^2
h	Heat transfer coefficient, W/m^2K
k	Thermal conductivity of the fluid, W/mK
L	Tube length, m
Nu	Nusselt number, $Nu = hD/k_0$
P	Pressure, Pa
Pr	Prandtl number, $Pr=C_p\mu_0/k$
q●	Wall heat flux, W/m^2
r	Radial coordinate, m
r_0	Tube radius, m
Re	Reynolds number, $Re=\rho_0 V_0 D/\mu_0$
S_m, S_e	Particles source terms in the base fluid equations
T	Fluid temperature, K
T*	Dimensionless temperature, $T^*=(T-T_w)/(T_b-T_w)$
V	Axial velocity, m/s
z	Axial coordinate, m

Greek letters

φ. .	Particle volume concentration
μ. .	Fluid dynamic viscosity, kg/ms

ρ. Fluid density, kg/m^3

τ. . Wall shear stress, Pa

Subscripts

av Average value

b Bulk value

bf Refers to base-fluid

nf Refers to nanofluid property

p Refers to particle property

r Refers to 'nanofluid/base-fluid' ratio

x x direction

w Value at wall tube

0 Refers to the reference (inlet) condition

1 INTRODUCTION

Convective heat transfer is very important for many industrial heating or cooling equipments. The heat convection can passively be enhanced by changing flow geometry, boundary conditions or by enhancing fluid thermophysical properties. An innovative way of improving the thermal conductivities of fluids is to suspend small solid particles in the fluid. Maxwell [1, 2] showed the possibility of increasing thermal conductivity of a mixture by more volume fraction of solid particles. These fluids containing colloidal suspended nanoparticles have been called nanofluids. Several investigations revealed that nanofluid heat transfer coefficient could be increased by more than 20% also in the case of very low nanoparticles concentrations [3, 4].

Nowadays there is a fast growth of research activities in this heat transfer area [5-9], because the impact of nanofluid technology is expected to be relevant considering that heat transfer performance of heat exchangers or cooling devices is fundamental in many industries [10]. Recently an industrial application was presented by Kulkarni et al. [11], that proposed aluminum oxide nanofluids as jacket water coolant in a diesel engine for electric generation, showing that the efficiency of waste heat recovery heat exchanger increased due to

nanofluid, because of its superior convective heat transfer coefficient. Moreover Nnanna et al. [12] developed a nanofluid heat exchanger for electronic cooling devices. They showed how the system performance improved with respect to conventional equipments.

It was demonstrated that solid nanoparticle colloids are extremely stable and exhibit no significant settling under static conditions, even after weeks or months [9, 13]. However, the development of nanofluids is still hindered by several factors such as the lack of agreement among experimental results from different research groups, poor characterization of suspensions and the lack of theoretical understanding of the heat transfer mechanisms [9]. Different concepts and models have been proposed to explain the enhancement of heat transfer [8, 14-17].

Theoretical and experimental investigations have been accomplished to estimate the effective thermal conductivity of nanofluids. Some experimental studies [18, 19] show that the measured thermal conductivity of nanofluids is much larger than the classical theoretical predictions [20]. Other experimental investigations [21, 22] revealed that the thermal conductivity has not shown any anomalous enhancement and for lower volume fractions, the results agree well with the classical equations [20, 23]. Many attempts have been made to formulate efficient theoretical models for the prediction of the effective thermal conductivity, but this topic is still seriously incomplete [24–26].

Relatively, few theoretical and experimental investigations have been reported on convective heat transfer in confined flows, as also reviewed in [7-9, 27].

Experimental results were obtained on convective heat transfer for laminar and turbulent flow of a nanofluid inside a tube in [14, 28, 29]. Correlations for the Nusselt number, using nanofluids composed of water and Cu, TiO_2 and Al_2O_3 nanoparticles were proposed. Enhancement of heat transfer performance over the base fluid for the assigned Reynolds number is observed. Experimental results for the convective heat transfer of Al_2O_3 (27–56 nm)/water based nanofluids flowing through a copper tube in laminar regime was reported in [30]. It was observed that the improvement of the heat transfer coefficient is particularly large at the entrance region, and it decreases with the axial distance. The heat transfer performance of CNT nanofluids in a tube was investigated

in [31]. Results showed that the enhancement of heat transfer coefficient is significantly higher than the increase in the effective thermal conductivity.

Numerical investigations on nanofluids are carried out using two approaches. The first approach assumes that the continuum assumption is still valid for fluids with suspended nanosize particles, while the other approach considers a two-phase model for better description of both the fluid and the solid phases. Another approach is to adopt the Boltzmann theory.

The single phase model with physical and thermal properties, all assumed to be constant with temperature, was employed in [32-35]. The hydrodynamic and thermal characteristics of nanofluids, flowing through a uniformly heated tube, in both laminar and turbulent regimes with adjusted properties, was investigated in [32]. The advantages of nanofluids with respect to heat transfer were discussed in [33], but it was also found that the inclusion of nanoparticles introduced drastic effects on the wall shear stress. A new correlation was proposed in [34] to describe the thermal performance of Al_2O_3-water nanofluids under turbulent regime and a numerical study of heat transfer for water–Al_2O_3 nanofluids in a radial cooling system was accomplished in Roy et al. [35]. They found that addition of nanoparticles in the base fluid increases the heat transfer rates considerably. Laminar forced convection flow of nanofluids between two coaxial and parallel disks with central axial injection was considered using temperature dependent nanofluid properties in [36]. The single phase flow model was solved numerically. Results have shown that considerable differences are obtained when using constant property nanofluids with respect to nanofluids with temperature dependent properties. It has been found that to an increase in wall heat flux corresponds an increase in the average heat transfer coefficient whilst the wall shear stress decreases when temperature-dependent nanofluid properties are used. A numerical study on fully developed laminar mixed convection of a nanofluid consisting of water and Al_2O_3 in a horizontal curved tube was carried out in [37]. Three-dimensional elliptic governing equations were used and the single phase model was employed. It was observed that the fraction of nanoparticles volume does not have a direct effect on the secondary flow, axial velocity and the skin friction coefficient. For a given Reynolds number, a negative effect of buoyancy force on the Nusselt number is obtained while the concentration of nanoparticles has a positive effect on the heat transfer enhancement and also on the reduction of skin friction.

The conjugate heat transfer problem for microheat sinks, considering two types of nanofluids, was numerically investigated in [38]. The effect of Brownian motion on the effective fluid viscosity was considered and found to be less significant than that on the effective thermal conductivity. A numerical investigation on the cooling performance of a microchannel heat sink with nanofluids was carried out in [39]. A theoretical model of thermal conductivity of nanofluids that accounts for the fundamental role of Brownian motion was used. Results showed that nanofluids reduced both the thermal resistance and the temperature difference between the heated microchannel wall and the coolant.

The two phase approach seems a better model to describe the nanofluid flow. In fact, the slip velocity between the fluid and particles might not be zero [14] due to several factors such as gravity, friction between the fluid and solid particles, Brownian forces, Brownian diffusion, sedimentation and dispersion. The two-phase approach provides a field description of the dynamics of each phase or, alternatively, the Lagrangian trajectories of individual particles coupled with the Eulerian description of the fluid flow field [40, 41]. A two phase mixture model was applied to study the turbulent forced convection flow of a nanofluid in a uniformly heated tube [42] and more recently Namburu et al. [43] investigated the turbulent convection flow of nanofluids inside a tube considering variable properties.

In this paper, developing laminar forced convection flow of a nanofluid in a circular tube is numerically investigated. Steady state of a two dimensional axial symmetric flow is considered and the circular tube is heated at uniform heat flux. The study is carried out for water with alumina particles with a spherical size of 100 nm diameter. The CFD commercial code, Fluent [44], is employed to solve the problem by means of finite volume method. Single phase and discrete phase approaches are employed to evaluate the developing laminar forced convection flow, taking the constant and temperature variable thermophysical properties into account. A comparison between results obtained by two different models is accomplished in terms of temperature and velocity distributions and Nusselt number profiles. The numerical simulation results are also compared with experimental data of Wen and Ding [30] and Heris et al. [45].

The aim of this paper is just to test the response of this model, evaluating its performance with smaller particles, because it has the great advantage to require just the thermophysical properties of the base fluid and

particles as input. Nothing is required about the whole mixture, so it could be used as a first step analysis to check the performance of a new nanofluid.

2 MATHEMATICAL MODELLING

Figure 1a shows the geometrical configuration under consideration. It consists of a tube with a length (L) of 1.0 m and a diameter (D) of 0.01 m. The nanofluid considered is composed of water and Al_2O_3 particles. The fluid enters with uniform temperature and axial velocity profiles at the inlet section. The tube has appropriate length in order to obtain fully developed profiles (velocity and thermal) at the outlet section (L/D=100). The condition of the axially and circumferentially uniform wall heat flux is considered in this study. Also, the flow and the thermal field are assumed to be symmetrical with respect to the vertical plane passing through the tube main axis so that half of the tube is considered.

The single phase model, which has been used frequently for nanofluids, is also implemented to compare its predictions with the mixture model. The following equations represent the mathematical formulation of the single phase model [32-36, 43, 46] and of the continuous phase of the two-phase model [46, 47]:

Conservation of mass:

$$div(\rho \vec{V}) = 0 \tag{1}$$

Momentum equation:

$$div(\rho \vec{V} \vec{V}) = -gradP + \nabla \cdot \left(\mu \nabla \vec{V} \right) + S_m \tag{2}$$

Energy equation:

$$div(\rho \vec{V} CpT) = div(kgradT) + S_e \tag{3}$$

The compression work and the viscous dissipation are assumed negligible in the energy equation; the source/sink terms S_m and S_e represent the integrated effects of momentum and energy exchange with base fluid, as shown in the following, and they are equal to zero in the case of single phase model.

Discrete phase is made of spherical particles following the model given by Ounis et al. [48]. Accordingly, motion equation is expressed in a Lagrangian form, to obtain the following expression [46-48]:

$$\frac{d\vec{V}_p}{dt} = F_D(\vec{V} - \vec{V}_p) + \frac{\vec{g}(\rho_p - \rho)}{\rho_p} + \vec{F} \tag{4}$$

where F is an additional term that can eventually include important additional forces under determined circumstances (i.e. forces that arise due to rotation of reference frame, thermophoretic force, Brownian force), F_D ($\mathbf{V}$ -$\mathbf{V}_p$) is resistance force per particle mass unit. Eq. (4) has a general validity, because it is simply the expression of a force balance on a particle immersed in a fluid. To solve Eq. (4a), it needs to specify the drag coefficient F_D and it can be done using the Stokes' law. At this point a first limitation is imposed to the model, because the Stokes' law is valid for $Re_d \leq 0.1$ [49], where Re_d is defined as:

$$\mathrm{Re}_d = \frac{\rho_{0,bf} \cdot d \cdot V_{0,av}}{\mu_{0,bf}} \tag{5a}$$

In the cases considered in the present work $Re_p \approx 0.01$, so the following form of the Stokes resistance law is considered [46, 48, 49]:

$$F_D = \frac{18\mu_{bf}}{d^2 \rho_p C_c} \tag{5b}$$

The factor C_c is the Cunningham correction [46, 48]:

$$C_c = 1 + \frac{2\lambda}{d}\left(1.257 + 0.4e^{(1.1d/2\lambda)}\right) \tag{5c}$$

where λ is the particle mean free path. Cunningham correction is necessary to apply the Stokes' resistance law to submicrometer particles [46, 48].

Once solved Eq. (4), it is possible to evaluate the momentum transfer between particles and base fluid, computed by examining the change in momentum of a particle as it passes through each control volume in the model. This momentum change is calculated as [44, 47]:

$$S_m = \sum_{np} \frac{m_p}{\delta V} \frac{d\vec{V}_p}{dt} \tag{2a}$$

where δV is the cell volume and np is the number of particles within a cell volume and those cells with np=0 are assigned a zero value for the source terms.

The same approach used for momentum equation can be employed for energy equation and for spherical particles the following equation is obtained [46, 47]:

$$\rho_p Cp_p \frac{dT_p}{dt} = \frac{6h}{d}\left(T - T_p\right) \tag{6}$$

where h is calculated from the Ranz and Marshall correlation [50, 51]:

$$Nu = \frac{h \cdot d}{k_{bf}} = 2.0 + 0.6 \cdot \mathrm{Re}_d^{1/2} \cdot \mathrm{Pr}^{1/3} \tag{6a}$$

valid for $1<Re_d \cdot Pr^{2/3}<5 \cdot 10^4$, where Re_d is defined in Eq. 5a.

Following the same approach used for the momentum equation, it is now possible to calculate the source term, S_e, for the energy equation [44, 47]:

$$S_e = \sum_{np} \frac{m_p}{\delta V} Cp \cdot \frac{dT_p}{dt} \tag{3a}$$

The main approximation of the DPM model applied to the nanoparticles is represented by the Ranz and Marshall correlation, which was developed for submicrometer particles and, moreover, in the present case Re_d is slightly outside from the lower limit, being around 0.5.

2.1 Boundary conditions

At the tube inlet, profiles of uniform axial velocity V_0, temperature T_0 (=293 K) prevail. Moreover, in the case of temperature dependent properties, the reference viscosity value for Re calculation is taken at T_0. At the tube exit section, the fully developed conditions prevail, that is to say that all axial derivatives are zero. No-slip conditions and uniform heat flux are imposed on the tube wall. As noted earlier, both the flow and thermal fields are assumed symmetrical with respect to the vertical plane passing through the tube main axis.

2.2 Physical properties of the nanofluids for single phase model approach

The determination of nanofluid properties is, as previously mentioned, at the center of current nanofluid research. Base nanofluid properties have been published over the past few years. However, only recently have

some data on temperature-dependent properties been provided, even though they are only for nanofluid effective thermal conductivity and effective absolute viscosity and for a few particle loadings.

For single phase model, the following formulas were used to compute the thermal and physical properties of the considered nanofluid:

Density

In the absence of experimental data for nanofluid densities, constant-value temperature independent values, based on nanoparticle volume fraction, are used:

$$\rho_{nf} = (1-\varphi)\rho_{bf} + \varphi\rho_p \tag{7}$$

Specific heat

Similarly, in the absence of experimental data relative to nanofluids, it has been suggested that the effective specific heat can be calculated using the following equation as reported in [28, 32-36, 46]:

$$Cp_{nf} = (1-\varphi)Cp_{bf} + \varphi Cp_p \tag{8a}$$

Other authors suggest an alternative approach based on heat capacity concept [13,15]:

$$(\rho Cp)_{nf} = (1-\varphi)(\rho Cp)_{bf} + \varphi(\rho Cp)_p \tag{8b}$$

These two formulations may of course lead to different results for specific heat. Due to the lack of experimental data, both formulations can be considered equivalent in estimating nanofluid specific heat capacity [36]. Moreover the difference in the Cp calculation using the two approach is less than 10% for the cases considered in this present work. In this paper, Eq. (8a) is considered for the calculations.

Dynamic viscosity

In this work, dynamic viscosity dependence only on φ is considered in one case, then the variability with the temperature is taken into account in the other case.

In the first case, in order to evaluate nanofluid dynamic viscosity, a least-square curve fitting, based on some scarce experimental data available in [17, 52, 53] was performed by Maiga et al. [32, 33], leading to the following equation:

$$\mu_r = \frac{\mu_{nf}}{\mu_{bf}} = 123\varphi^2 + 7.3\varphi + 1 \tag{9a}$$

In the second case it is assumed that temperature dependant nanofluid properties will yield even better predictions with respect to constant properties. In the present work, the dynamic viscosity is evaluated by means of the polynomial curve fitting proposed in [36], based on the data reported in [54]. The resulting equations were used to compute the nanofluid effective viscosity, as a function of the local temperature, expressed in K as given in [36]:

$$\varphi = 1\% \rightarrow \mu_{nf} = 3.4 \cdot 10^{-2} - 1.975 \cdot 10^{-4} T + 2.912 \cdot 10^{-7} T^2$$

$$\varphi = 4\% \rightarrow \mu_{nf} = 4.051 \cdot 10^{-2} - 2.353 \cdot 10^{-4} T + 3.475 \cdot 10^{-7} T^2 \tag{9b}$$

Thermal conductivity

For the thermal conductivity determination, the same criteria used for the dynamic viscosity is considered, thereby introducing the following equations, as given in [32, 33]:

$$k_r = \frac{k_{nf}}{k_{bf}} = 4.97\varphi^2 + 2.72\varphi + 1 \tag{10}$$

obtained using the model proposed by [20], assuming spherical particles. Such model, which was first developed based on data from several mixtures containing relatively large particles (i.e. millimeter and micrometer size particles) is believed to be acceptable for use with nanofluids, although it may give underestimated values of thermal conductivity [32, 33].

In the second case, temperature dependent thermal conductivity is determined by the equation suggested in [36], derived from the experimental data given in [54]. The following equations, with T in K, are considered [36]:

$$\varphi = 1\% \rightarrow k_{nf} = 0.003352 \cdot T - 0.3708$$

$$\varphi = 4\% \rightarrow k_{nf} = 0.004961 \cdot T - 0.8078 \tag{11}$$

For two phase model, the thermophysical properties of Al_2O_3 are:

ρ_p=3880 kg/m^3; Cp_p=773 J/(kg K); k_p=36 W/(m K)

For the first case, the thermophysical properties of base fluid are:

ρ_{bf}=998.2 kg/m^3; Cp_{bf}=4182 J/(kg K); k_{bf}=0.597 W/(m K); μ_{bf}=9.93x10^{-4} kg/(m s)

For the second case, the thermophysical properties of base fluid, with T expressed in K, are:

$$k_{bf} = -1.13 + 9.71 \cdot 10^{-3} T - 1.31 \cdot 10^{-5} T^2 \quad (12)$$

$$\mu_{bf} = 7.57 \cdot 10^{-2} - 6.37 \cdot 10^{-4} T + 1.80 \cdot 10^{-6} T^2 - 1.73 \cdot 10^{-9} T^3 \quad (13)$$

where ρ and Cp are independent of temperature and equal to the previous value.

2.3 Numerical method

The computational fluid dynamic code FLUENT [44] is employed to solve the present problem. The governing equations (1-3) are solved by control volume approach. This method is based on the spatial integration of the conservation equations over finite control volumes, converting the governing equations to a set of algebraic equations. The algebraic "discretized equations", resulting from this spatial integration process, are sequentially solved throughout the physical domain considered. FLUENT solves the systems resulting from discretization schemes using a numerical method. The residuals resulting from the integration of the governing equations (1-3) are considered as convergence indicators.

In order to ensure the accuracy as well as the consistency of numerical results, several non-uniform grids were subjected to an extensive testing procedure for each of the cases considered.

Results obtained for a particular test case showed that, for the tube flow problem under consideration, the 10 x 12 x 400 non-uniform grid appears to be satisfactory to ensure the precision of numerical results as well as their independency with respect to the number of nodes used. Such grid has 10, 12 and 400 nodes along the radial, tangential and axial directions respectively, with highly packed grid points in the vicinity of the tube wall, especially at the entrance region.

The computer model has been successfully validated with correlation reported in [55] for thermally and hydraulically developing flow, showing an average error less than 2%, as reported in Fig. 1b, where local Nusselt number is calculated according to the following definition:

$$Nu(z) = \frac{h(z) \cdot D}{k_0} \tag{14}$$

and h(z) is defined as:

$$h(z) = \frac{q}{T(z)_w - T(z)_b} \tag{15}$$

From the previous equation the $\overline{h}$ is calculated as follow:

$$h_{av} = \frac{1}{L}\int_0^L h(z)dz \tag{16}$$

and the average Nusselt number is defined as:

$$Nu_{av} = \frac{h_{av} \cdot D}{k_0} \tag{17}$$

3 RESULTS

Results were carried out employing the single phase and discrete phase models for φ=1% and 4%, Re=250, 500, 750 and 1050 and q=5000, 7500 and 10000 W/m^2 for both constant and temperature-dependent properties. In all cases, the size of the spherical particles is considered equal to 100 nm.

Figure 2a shows the profiles of axial velocity along tube radius up to z/L=0.2 for Re=250, q=5000 W/m^2 and φ=4%. It can be observed that nanofluid motion is fully developed at exit section which is located 1.00 m after the inlet section. For single phase model, when properties are not dependent on temperature, velocity profile and hydrodynamic entrance length are nearly independent on concentration value. Velocity axial profiles are nearly identical at z/L=0.2 for φ=0%, 1% and 4%, as shown in Fig. 2b.

Thermal entrance length depends on Prandtl number too, so when concentration increases Pr number also increases and consequently, thermal entrance length becomes greater. Dimensionless temperature of the fluid at several axial locations along the radius is reported in Fig.3 for φ=0% and 4%. For both the base fluid and the nanofluid, the motion is not thermally developed. As the concentration increases the thermal entrance length

rises, as it is also noticed by a higher slope of relative local heat transfer coefficient, h_r, for φ=4% shown in Fig. 4a.

This figure also clearly shows the enhancement of convective heat transfer due to the presence of nanoparticles. At the exit section, the increment of the heat transfer coefficient is 14% for constant properties and 17% for temperature dependent properties, in the case of φ=4%.The advantage is particularly great at the entrance section.

Relative local coefficient is always decreasing with axis location when fluid properties are constant, whereas temperature-dependent properties make h_r to increase with z. This happens because, in the case of temperature dependent properties, there is a linear increase of thermal conductivity with temperature, and therefore, a better heat transfer between wall and fluid exists. Consequently, there is a decrease in the temperature difference between the wall and bulk temperature and with the heat flux on the wall being constant, there is an increase in the heat transfer coefficient, as shown in Figs. 4b and 4c.

From Fig. 4a, in the case of temperature dependent properties, it is possible to observe an increase in the curves slopes, which is due to the fact that the increase in h_{nf} is greater than h_{bf}. If the two coefficients (h_{nf} and h_{bf}) had the same increase, the curves of Fig. 4a for constant and temperature dependent properties would have overlapped.

The case with variable properties presents, with respect to the case with constant properties, the ratio h_{nf}/h_{bf} with a larger increase because the thermal conductivity of the nanofluid has a higher increment than the simple water.

In Fig. 5a and b radial temperature profiles at z/L=1.0 for Re=250 and q=5000 W/m^2 are reported for the investigated models for constant and non-constant properties respectively. For constant properties, Fig. 5a, temperature is strongly dependent on concentration φ. When concentration increases fluid temperature decreases quickly, particularly near the tube wall; furthermore, the difference between temperature values, for base fluid and for nanofluid, increases as r increases, indicating that higher heat transfer rate, with nanoparticles, is achieved. For φ=1%, two phase model gives lower temperatures than single phase model for $r/r_0<0.15$. Moreover, the difference between temperature at the axis ($r/r_0=0$) and surface ($r/r_0=1$) is lower for

two-phase model. When the volume concentration of particles is higher (4%), temperature profile for two-phase model is very similar to the one for single phase model and, on the surface, there is a temperature increase with respect to the reference value of 29 K in both models. When properties are temperature-dependent, Fig.5b, for φ=1%, temperatures difference between the two models decreases with respect to the case of constant properties and at tube wall, the temperature for two phase model is about 1 K lower than the one for single phase model. Moreover, in the core region ($r/r_0<0.2$) there is a clear existence of a uniform temperature fluid zone that becomes more visible for higher value of φ.

Figures 6a and b show wall and bulk temperature profiles along tube axis for Re=250 and q=5000 W/m^2 for the single and two phase models and for constant and variable properties respectively. It can be noticed that the decrease of wall and bulk temperatures for a nanofluid, with respect to the base fluid, increases with the z coordinate. For a concentration of 1%, wall and bulk temperatures for the single phase model are higher than the ones for the two-phase model, whereas for φ=4%, temperature profiles for the two models are very similar particularly for constant properties.

These results have indicated the beneficial effects due to nanoparticles effects that may be mainly explained by the fact that, with the presence of such particles, the thermal properties of the resulting mixture have considerably improved, moreover additional effects such as gravity, drag on the particles, diffusion, Brownian forces play an important role [46]. In fact considering temperature constant properties, in the single phase model such effects are not considered and the increase in the average heat transfer coefficient is very similar to that of nanofluid vs. base fluid thermal conductivity. While, in the case of discrete phase model, where gravity and drag are taken into account, there is a higher increase of the average heat transfer coefficient, especially for φ=1%, as shown in Fig. 7a. Therefore, the nanofluid offers, as expected, higher thermal capability than the base fluid. It is also noted that with higher thermal conductivity of the mixture, the convective heat transfer between wall and fluid should consequently be more efficient.

Average heat transfer coefficient and Nusselt number are reported in Table 1 together with the relative increase of the total heat transfer rates and Nusselt number as a function of the nanoparticle volume fraction φ. As can be noticed, significant increases of the total heat transfer rates can be found with the use of suspended

nanoparticles. For example, for φ = 4%, heat transfer rate and Nusselt number increase of about 20% and 16% respectively. Slight discrepancies are noticed between the models.

Table 2 presents the average wall shear stress value, τ_{av}, and the nanofluid-to-base fluid wall shear stress ratio (defined as $\tau_r = \tau_{nf}/\tau_{bf}$) for the case Re =250 and q=5000W/m^2 and various particle concentrations. For pure water, τ_{av} value is lower when properties are temperature-dependent because viscosity decreases with temperature. When φ=1%, τ_{av} values for constant properties are higher than those for variable properties and in both cases τ_{av} values, for two-phase model are higher than those for single phase model. When φ=4%, τ_{av} values for constant properties are again higher than those for variable properties, whereas τ_{av} values for two-phase model are lower than those for single phase model. However, the difference between the values for single and two-phase models is small. The values of $\tau_{r,}$ for φ=1%, are similar for the single and two-phase models, whereas for φ=4%, all the four models give very similar values.

Relative heat transfer coefficients are reported in table 3 for the investigated models, for the same Reynolds number (Re=250) and different heat fluxes (q=5000, 7500 and 10000W/m^2). The coefficients h_r in the case of φ=1% and 4% and for non-dependent temperature properties are practically constant with heat flux and, although the coefficients are very similar, in the single phase model, they tend to increase slightly when properties are temperature dependent, while for the two-phase model, the coefficients do not change with the heat flux, but they result slightly higher when properties are constant. An analogous behaviour is observed for the relative wall shear stress τ_r, as shown in Table 4. Wall shear stress decreases with heat flux in all the investigated cases because when heat transfer increases, bulk temperature rises too hence fluid viscosity decreases. As previously noticed the presence of nanoparticles increases the wall shear stress. For φ=1%, τ_r is almost constant with heat flux, whereas for φ=4%, τ_r slightly increases with q.

In general, τ_r increases considerably with the particle volume fraction, φ, and this adverse effect is somehow expected, as it results from a strong increase of the mixture viscosity due to inclusion of nanoparticles.

The effect of Reynolds number on average heat transfer coefficient is shown in Figures 7a and b for the single and two phase model, at q=10000 W/m^2. When the properties are constant, Fig.7a, for φ=1%, some differences, in the range of about 8%-11%, are detected between the single and two phase model, particularly,

the two phase model which leads to overestimated values. When the concentration increases, these differences tend to reduce. In fact, for φ=4% they are in the range of about 2%-7%, with the highest deviation for Re=1050. When properties are temperature-dependent, Fig. 7b, the differences between the single and two phase models reduce for both examined concentrations. In fact when φ=1%, the differences between the two models are contained between 4% and 8%, while for φ=4%, they are between 2% and 4%, with the highest deviation always for Re=1050.

In Fig. 8a and b, Nusselt number as function of Re for the considered concentrations is reported. In the figure a comparison with the correlation given by Maiga et al. [33] and the experimental data of Heris et al. [45] is also carried out. In Fig. 8a it is possible to observe the Nu_{av} behaviour for φ=1% and, except for Re=250, a good agreement is found with the correlation given in [33]. Moreover, a maximum deviation of about 17%, in the case of Re=1050, for the single phase model, is estimated. The experimental data presented in [45] are obtained for a tube with constant wall temperature, they are therefore corrected by means of a 20% increase in Nussult number. This correction derives from the fact that Nu number in a developing laminar flow in a circular tube is averagely 20% higher for constant heat flux boundary condition with respect to constant temperature [56].

The corrected data given in [45] are very close to the ones obtained with the single phase model and constant properties with an error of 2.3% and 0.1%, respectively, for Re=500 and 750.

In Fig. 8b, average Nusselt number for φ=4% is shown and also in this case, except for Re=250, a good accord with the correlation given in [33] is confirmed. In fact, the maximum deviation is equal to 12% for Re=750 and single phase model with constant properties.

Finally, a comparison with the experimental data from Wen and Ding [30] is carried out for Re=1050 for φ=1%. In Table 5, local Nusselt number and its ratio with local Nusselt number for base fluid are reported at z/D = 26 and 63 and for all the investigated models. The lower differences between experimental and numerical data are for two-phase model with temperature-dependent properties, the maximum gap being equal to 3.5% at z/D=63.

4 CONCLUSIONS

In this paper the hydrodynamic and thermal behaviours of water-Al_2O_3 nanofluids flowing inside a uniformly heated tube were numerically investigated in stationary conditions and for laminar flow. Four models were employed: single and two-phase models with either constant or temperature-dependent properties.

Results clearly showed that the inclusion of nanoparticles produced a considerable increase of the heat transfer with respect to that of the base liquid. Heat transfer enhancement was increasing with the concentration of particle volume. However it was accompanied by increasing wall shear stress values.

It can be said that temperature dependent models present higher values of heat transfer coefficients and Nusselt numbers because the difference between wall and bulk temperature is minimized, thereby maximizing the heat transfer. On the other hand, another positive effect is due to the decrease of shear stress, because viscosity decreases with temperature.

For each investigated concentration value, the heat transfer enhancement is higher for the greatest Reynolds number. The effect of Reynolds number is greater for temperature dependent properties. A good relationship was shown with the data from Wen and Ding [27], Maiga et al. [33] and Heris et al. [45].

As for the comparison between single and two phase models, their results are quite similar (the maximum difference detected is 11% for the average heat transfer coefficient), especially for φ=4% and in the case of variable properties. In our opinion, this is a good result, as this model could be used to test new nanofluids, since it requires information about just particles and base fluid, with no reference to the mixture. Therefore,it may result as a “winning first glance” approach in the study of new mixtures, considering also the low cost connected to it.

ACKNOWLEDGMENTS

This work was supported by MIUR with Articolo 12 D. M. 593/2000 Grandi Laboratori “EliosLab”.

REFERENCES

[1] J.C. Maxwell, Electricity and Magnetism, Clarendon Press, Oxford, 1873.

[2] J.C. Maxwell, A Treatise on Electricity and Magnetism, Oxford University Press, Cambridge, 1881.

[3] Q. Li, Y. Xuan, Heat transfer enhancement of nanofluids, International Journal of Heat and Fluid Flow 21 (2000) 58-64.

[4] H.U. Kang, S.H. Kim, J.M. Oh, Estimation of thermal conductivity of nanofluid using experimental effective particle volume, Experimental Heat Transfer 19 (2006) 181-191.

[5] K. Khanafer, K. Vafai, M. Lightstone, Buoyancy-driven heat transfer enhancement in a two-dimensional enclosure utilizing nanofluids, International Journal of Heat and Mass Transfer 46 (19) (2003) 3639-3653.

[6] A.R.A. Khaled, K. Vafai, Heat transfer enhancement through control of thermal dispersion effects, International Journal of Heat and Mass Transfer 48 (11) (2005) 2172-2185.

[7] S.K. Das, S.U.S. Choi, H.E. Patel, Heat Transfer in Nanofluids-A Review, Heat Transfer Engineering 27 (10) (2006) 3–19.

[8] J. Buongiorno, Convective Transport in Nanofluids, ASME Journal of Heat Transfer 128 (2006) 240-250.

[9] X.Q. Wang, A.S. Mujumdar, Heat transfer characteristics of nanofluids: a review, International Journal of Thermal Sciences 46 (2007) 1–19.

[10] S.M.S. Murshed, K.C. Leong, C. Yang, Thermophysical and electrokinetic properties of nanofluids – A critical review, Applied Thermal Engineering 28 (2008) 2109-2125.

[11] D.P . Kulkarni, R.S. Vajjha, D.K Das, D. Oliva, Application of aluminum oxide nanofluids in diesel electric generator as jacket water coolant, Applied Thermal Engineering 28 (2008) 1774-1781.

[12] A.G.A. Nnanna, W. Rutherford, W. Elomar, B. Sankowski, Assessment of thermoelectric module with nanofluid heat exchanger, Applied Thermal Engineering, doi:10.1016/j.applthermaleng.2008.03.007

[13] J.A. Eastman, S.U.S. Choi, S. Li, G.. Soyez, L.J. Thompson, R.J. Di Melfi, Novel thermal properties of nanostructured materials, Material Science Forum 312-314 (1999) 629-634.

[14] Y. Xuan, Q. Li, Heat transfer enhancement of nanofluids, International Journal of Heat and Fluid Flow 21 (2000) 58–64.

[15] Y. Xuan, W. Roetzel, Conceptions for heat transfer correlations of nanofluids, International Journal of Heat and Mass Transfer 43 (2000) 3701–3707.

[16] P. Keblinski, S.R. Phillpot, S.U.S. Choi, J.A. Eastman, Mechanisms of heat flow in suspensions of nano-sized particles (nanofluid), International Journal of Heat and Mass Transfer 45 (2002) 855–863.

[17] X. Wang, X. Xu, S.U.S. Choi, Thermal conductivity of nanoparticle–fluid mixture, Journal of Thermophysics and Heat Transfer 13 (1999) 474–480.

[18] S.U.S. Choi, Z.G.. Zhang, W. Yu, F.E. Lockwood, E.A. Grulke, Anomalous thermal conductivity enhancement in nanotube suspension, Applied Physics Letters 79 (2001) 2252–2254.

[19] D.H. Yoo, K.S. Hong, H.S. Yang, Study of thermal conductivity of nanofluids for the application of heat transfer fluids, Thermochimica Acta 455 (2007) 66.

[20] R.L. Hamilton, O.K. Crosser, Thermal conductivity of heterogeneous two-component systems, I & EC Fundamentals, 1 (3) (1962) 187–191.

[21] S.A. Putman, D.G. Cahill, P.V. Braun, Z. Ge, R.G. Shimmin, Thermal conductivity of nanoparticle suspensions, Journal of Applied Physics 99 (2006) 084308.

[22] X. Zhang , H. Gu, M. Fujii, Effective thermal conductivity and thermal diffusivity of nanofluids containing spherical and cylindrical nanoparticles, Experimental Thermal Fluid Science 31 (2007) 593-599.

[23] E. Yamada, T. Ota, Effective thermal conductivity of dispersed materials, Wärme- und Stoffübetragung 13 (1980) 27-37.

[24] Q.Z. Xue, Model for effective thermal conductivity of nanofluids, Physics Letters A 307 (2003) 313–317.

[25] Y.M. Xuan, Q. Li, W. Hu, Aggregation structure and thermal conducting of nanofluids, AIChE Journal 49 (2004) 1038–1043.

[26] C.H. Chon, K.D. Kihm, S.P. Lee, S.U.S. Choi, Empirical correlation finding the role of temperature and particle size for nanofluid (Al2O3) thermal conductivity enhancement, Applied Physics Letters 87 (2005) 153107.

[27] W. Daungthongsuk, S. Wongwises, A critical review of convective heat transfer of nanofluids, Renewable and Sustainable Energy Reviews 11 (5) (2007) 797-817.

[28] B.C. Pak, Y.I. Cho, Hydrodynamic and heat transfer study of dispersed fluids with submicron metallic oxide particles, Experimental Heat Transfer 11 (1998) 151–170.

[29] Y.M. Xuan, Q. Li, Investigation on convective heat transfer and flow features of nanofluids, Journal of Heat Transfer 125 (2003) 151–155.

[30] D. Wen, Y. Ding, Experimental investigation into convective heat transfer of nanofluids at the entrance region under laminar flow conditions, International Journal of Heat and Mass Transfer 47 (24) (2004) 5181-5188.

[31] Y. Ding, H. Alias, D. Wen, R.A. Williams, Heat transfer of aqueous suspensions of carbon nanotubes (CNT nanofluids), International Journal of Heat and Mass Transfer 49 (2005) 240–250.

[32] S.E.B. Maiga, C.T. Nguyen, N. Galanis, G. Roy, Heat transfer behaviours of nanofluids in a uniformly heated tube, Superlattices Microstructures 35 (2004) 543–557.

[33] S.E.B. Maiga, S.J. Palm, C.T. Nguyen, G. Roy, N. Galanis, Heat transfer enhancement by using nanofluids in forced convection flows, International Journal of Heat and Fluid Flow 26 (4) (2005) 530–546.

[34] S.E.B. Maiga, N. Cong Tam, N. Galanis, G. Roy, T. Mare, M. Coqueux, Heat transfer enhancement in turbulent tube flow using Al2O3 nanoparticle suspension, International Journal of Numerical Methods in Heat and Fluid Flow 16 (3) (2006) 275–292.

[35] G. Roy, C.T. Nguyen, P.R. Lajoie, Numerical investigation of laminar flow and heat transfer in a radial flow cooling system with the use of nanofluids, Superlattices Microstructures 35 (2004) 497–511.

[36] S.J. Palm, G. Roy, C.T. Nguyen, Heat transfer enhancement with the use of nanofluids in radial flow cooling systems considering temperature dependent properties, Applied Thermal Engineering 26 (2006) 2209–2218.

[37] A. Akbarinia, A. Behzadmehr, Numerical study of laminar mixed convection of a nanofluid in horizontal curved tubes, Applied Thermal Engineering 27 (2007) 1327–1337.

[38] J. Koo, C. Kleinstreuer, Laminar nanofluid flow in micro-heat sinks, International Journal of Heat and Mass Transfer 48 (2005) 2652–2661.

[39] S.P. Jang, S.U.S. Choi, Cooling performance of a microchannel heat sink with nanofluids, Applied Thermal Engineering 26 (2006) 2457–2463.

[40] D. Gidaspow, Multiphase Flow and Fluidization, Academic Press, 1994.

[41] L.S. Fan, C. Zhu, Principle of Gas–Solid Flows, Cambridge University Press, 1998.

[42] A. Behzadmehr, M. Saffar-Avval, N. Galanis, Prediction of turbulent forced convection of a nanofluid in a tube with uniform heat flux using a two phase approach, International Journal of Heat and Fluid Flow 28 (2007) 211–219.

[43] P. K. Namburu, D. K. Das, K. M. Tanguturi, R. S. Vajjha, Numerical study of turbulent flow and heat transfer characteristics of nanofluids considering variable properties, International Journal of Thermal Sciences, doi:10.1016/j.ijthermalsci.2008.01.001

[44] Fluent 6.2 User Manual, Fluent Incorporated, 2006.

[45] S. Zeinali Heris, M. Nasar Esfahany, S. Gh. Etemad, Experimental investigation of convective heat transfer of Al_2O_3/water nanofluid in circular tube, International Journal of Heat and Fluid Flow 28 (2007) 203-210.

[46] S.K. Das, S.U.S. Choi, W. Yu, T. Pradeep, Nanofluids science and technology, John Wiley & Sons, Hoboken NJ, 2008

[47] W.J. Minkowycz, E.M. Sparrow, J.Y. Murthy, Handbook of numerical heat transfer, 2nd edition, John Wiley & Sons, Hoboken NJ, 2006

[48] H. Ounis, G. Ahmadi, J.B. McLaughlin, Brownian diffusion of submicrometer particles in the viscous sublayer, Journal of Colloid Interface Science 143 (1) (1991) 266-277.

[49] K. Asano, Mass Transfer - From fundamentals to modern industrial applications, WILEY-VCH Verlag GmbH & Co. KGaA, Weinheim, 2006.

[50] W. E. Ranz and W. R. Marshall, Jr. Evaporation from Drops, Part I. Chem. Eng. Prog., 48 (3) 141-146, March 1952.

[51] W. E. Ranz and W. R. Marshall, Jr. Evaporation from Drops, Part II. Chem. Eng. Prog., 48 (4) 173-180, April 1952.

[52] H. Masuda, A. Ebata, K. Teramae, N. Hishinuma, Alteration of thermal conductivity and viscosity of liquid by dispersing ultra-fine particles (dispersion of γ-Al_2O_3, SiO_2 and TiO_2 ultra-fine particles), Netsu Bussei (in Japanese) 4 (4) (1993) 227–233.

[53] S. Lee, S.U.S. Choi, S. Li, J.A. Eastman, Measuring thermal conductivity of fluids containing oxide nanoparticles, Journal of Heat Transfer 121 (1999) 280–289.

[54] N. Putra, W. Roetzel, S.K. Das, Natural convection of nanofluids, Heat and Mass Transfer 39 (2003) 775-784.

[55] S.W. Churchill, H. Ozoe, Correlations for forced convection with uniform heating in flow over a plate and in developing and fully developed flow in a tube, Journal of Heat Transfer 95 (1973) 78-84.

[56] A. Bejan, Convection Heat Transfer; 3 edition, John Wiley & Sons, New York, 2004.

FIGURE CAPTIONS

Figure 1. (a) geometrical configuration under study and (b) grid validation by means of Churchill and Ozoe correlation [55].

Figure 2. (a) profiles of axial velocity at several locations for Re=250, q=5000W/m^2 and φ=4% and (b) profiles of axial velocity at z=0.2m, for Re=250, q=5000W/m^2 and several concentration values.

Figure 3. Dimensionless temperature for Re=250 and q=5000 W/m^2 at several locations and for:

a) φ=0%; b) φ =4%.

Figure 4. (a) Increase in nanofluid heat transfer coefficient along tube axis for Re=250 and q=5000 W/m^2 for constant and variables properties, (b) heat transfer coefficient for constant properties, (c) heat transfer coefficient for temperature dependent properties.

Figure 5. Profiles of temperature along tube radius at z/L=0.99 for several concentrations and for Re=250 and q=5000 W/m^2:a) constant properties; b) variable properties.

Figure 6. Profiles of wall and bulk temperature along tube axis for several concentrations and for Re=250 and q=5000 W/m^2: a) constant properties; b) variable properties.

Figure 7. Average heat transfer coefficient as a function of Re for the single and two phase model for q=10000 W/m^2: a) constant properties; b) variable properties.

Figure 8. Nusselt number as function of Re for a) φ=1% and b) φ =4%.

Figure 1a

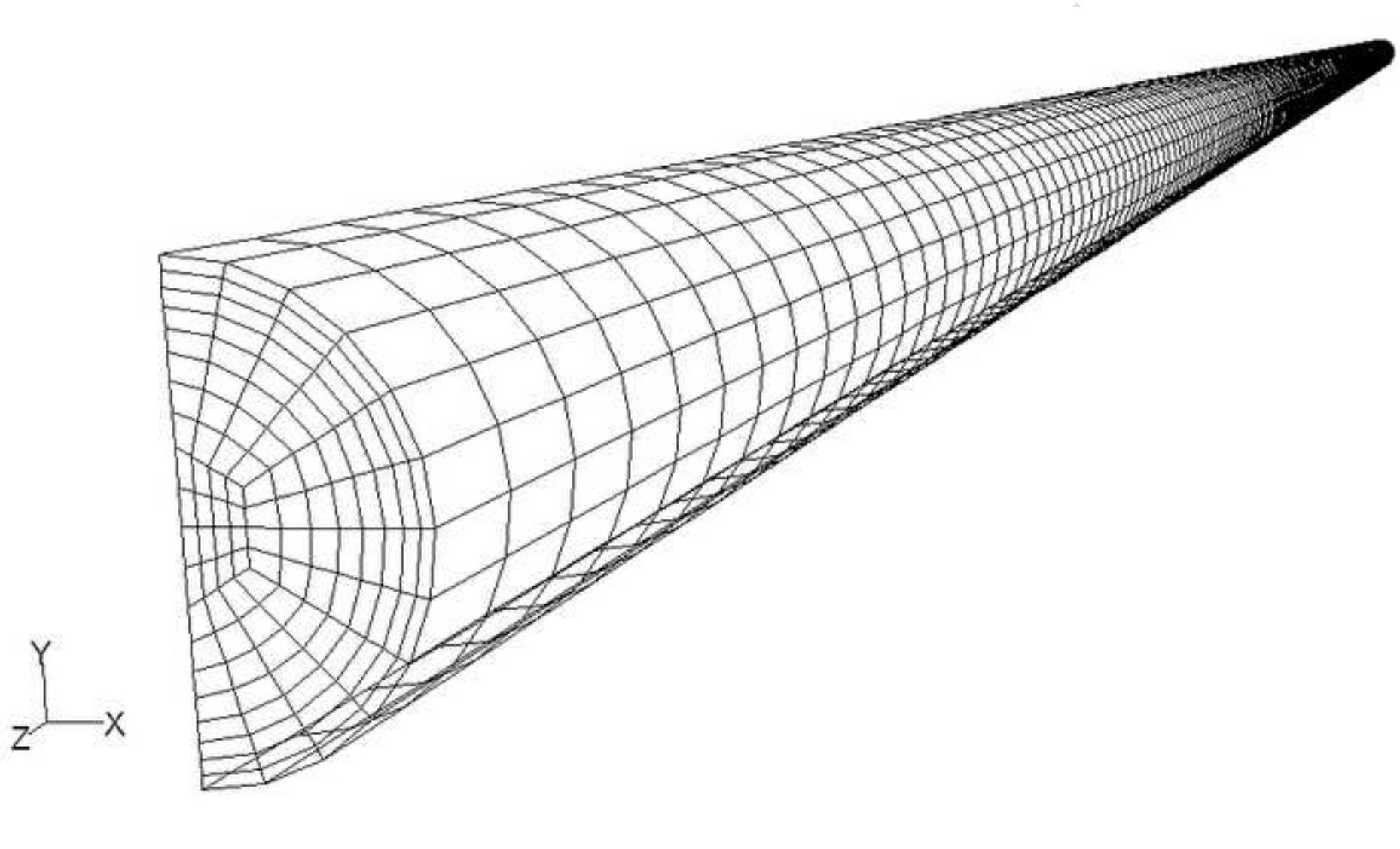

Figure 1b

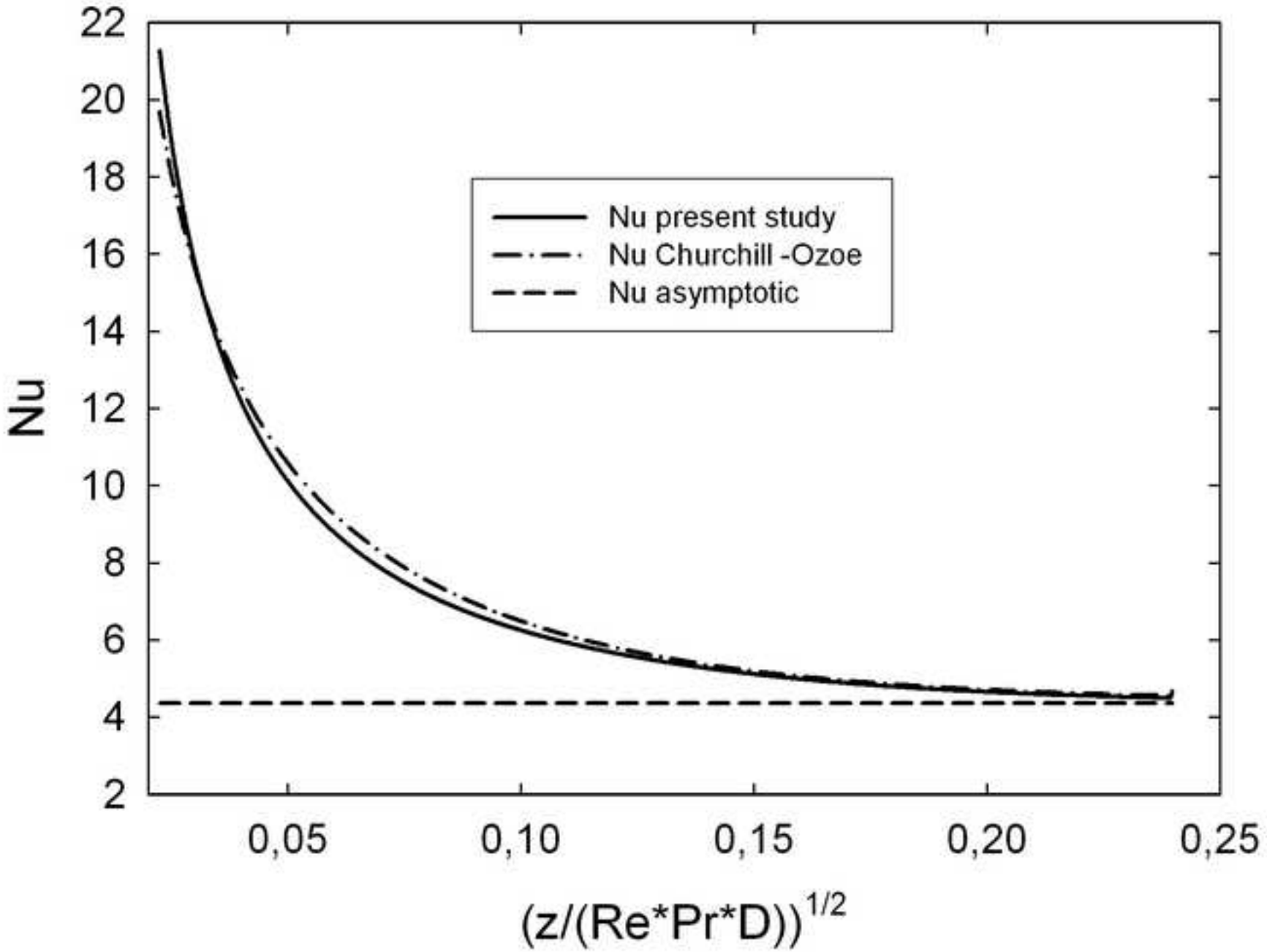
Nu present study
Nu Churchill -Ozoe
Nu asymptotic
Nu
22
20
18
16
14
12
10
8
6
4
2
0,05
0,10
0,15
0,20
0,25
(z/(Re*Pr*D))^1/2

Figure 2a

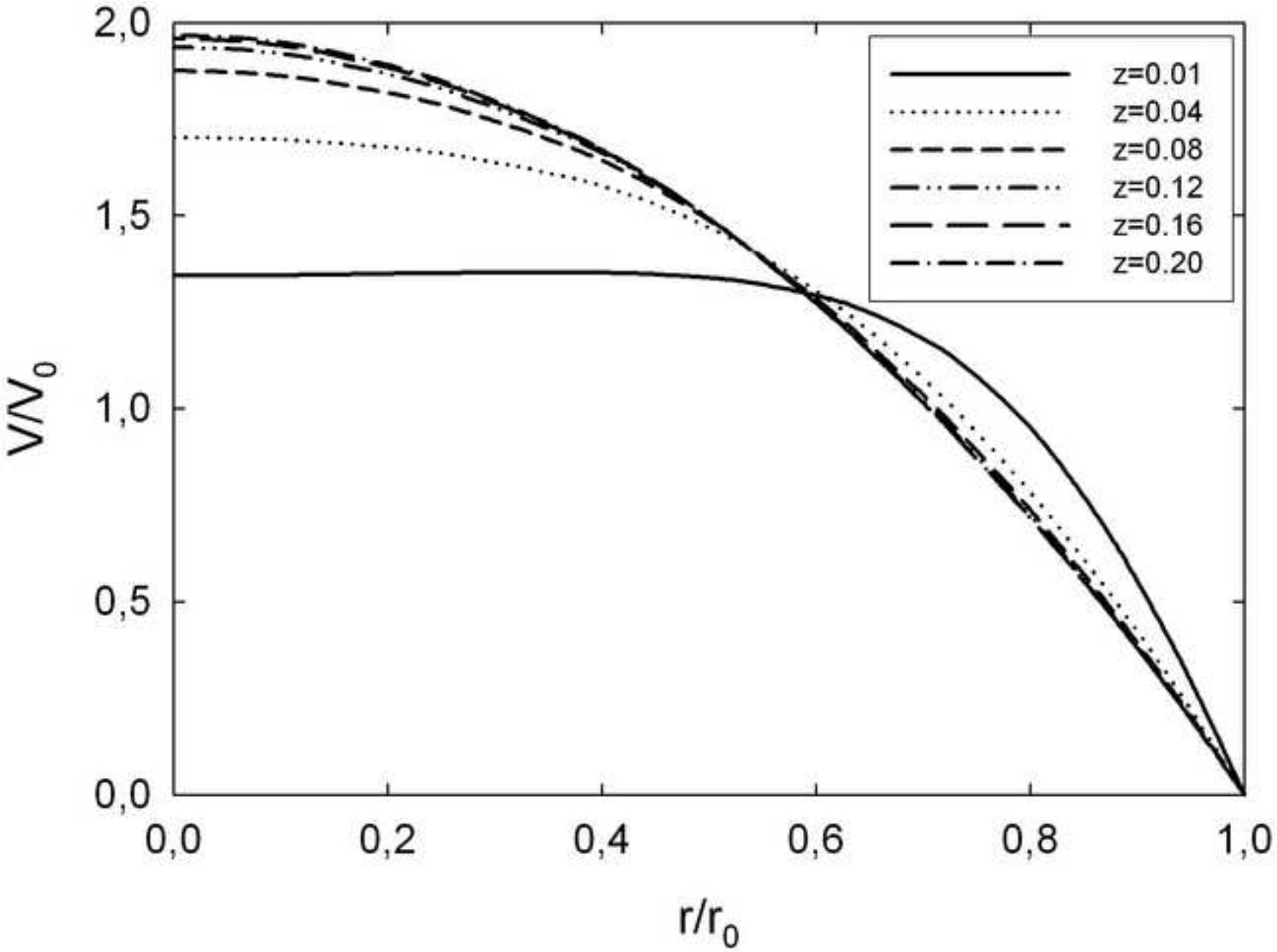
2,0
1,5
1,0
0,5
0,0
V/V0
0,0
0,2
0,4
0,6
0,8
1,0
r/r0
z=0.01
z=0.04
z=0.08
z=0.12
z=0.16
z=0.20

Figure 2b

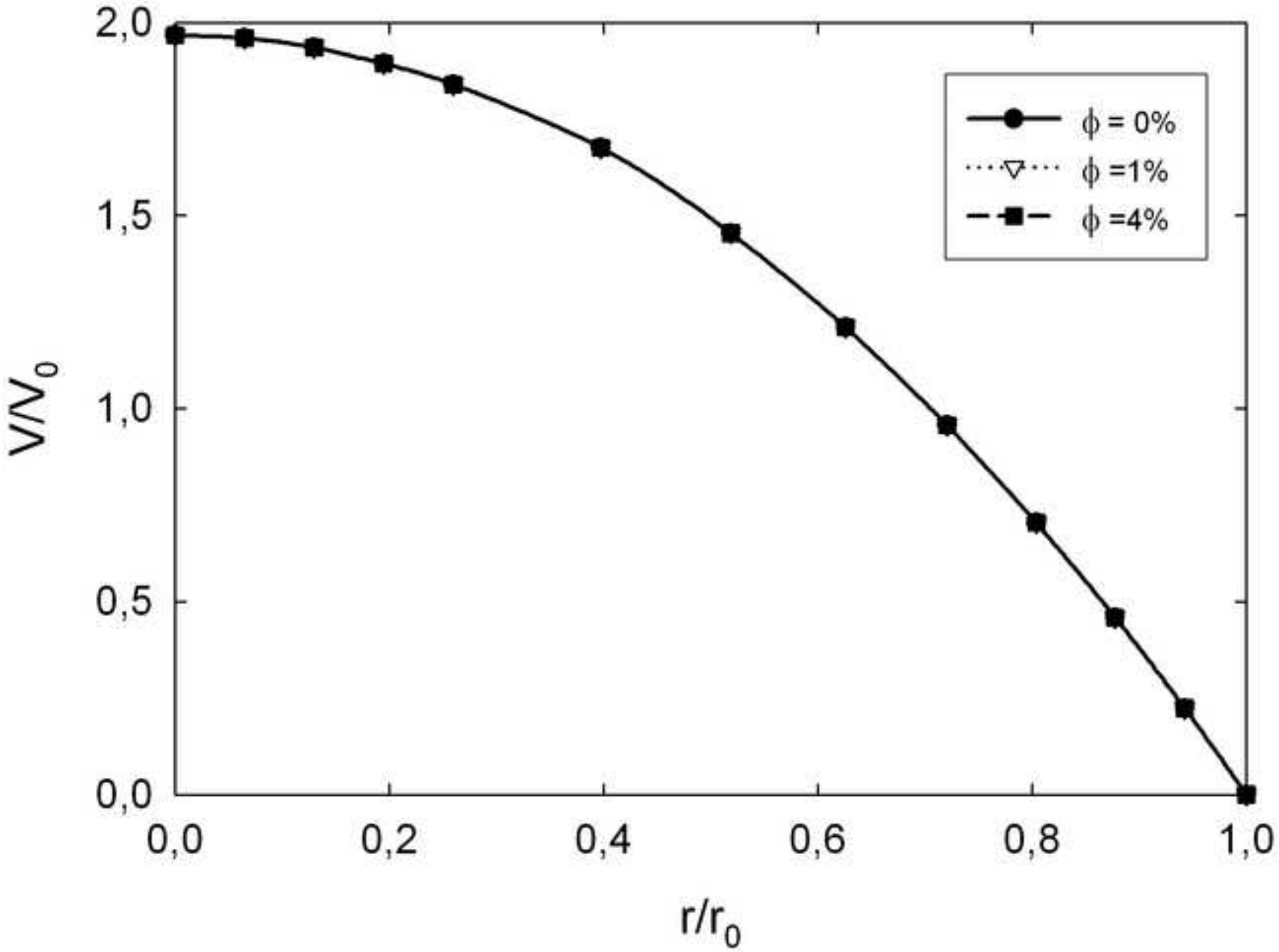

Figure 3a

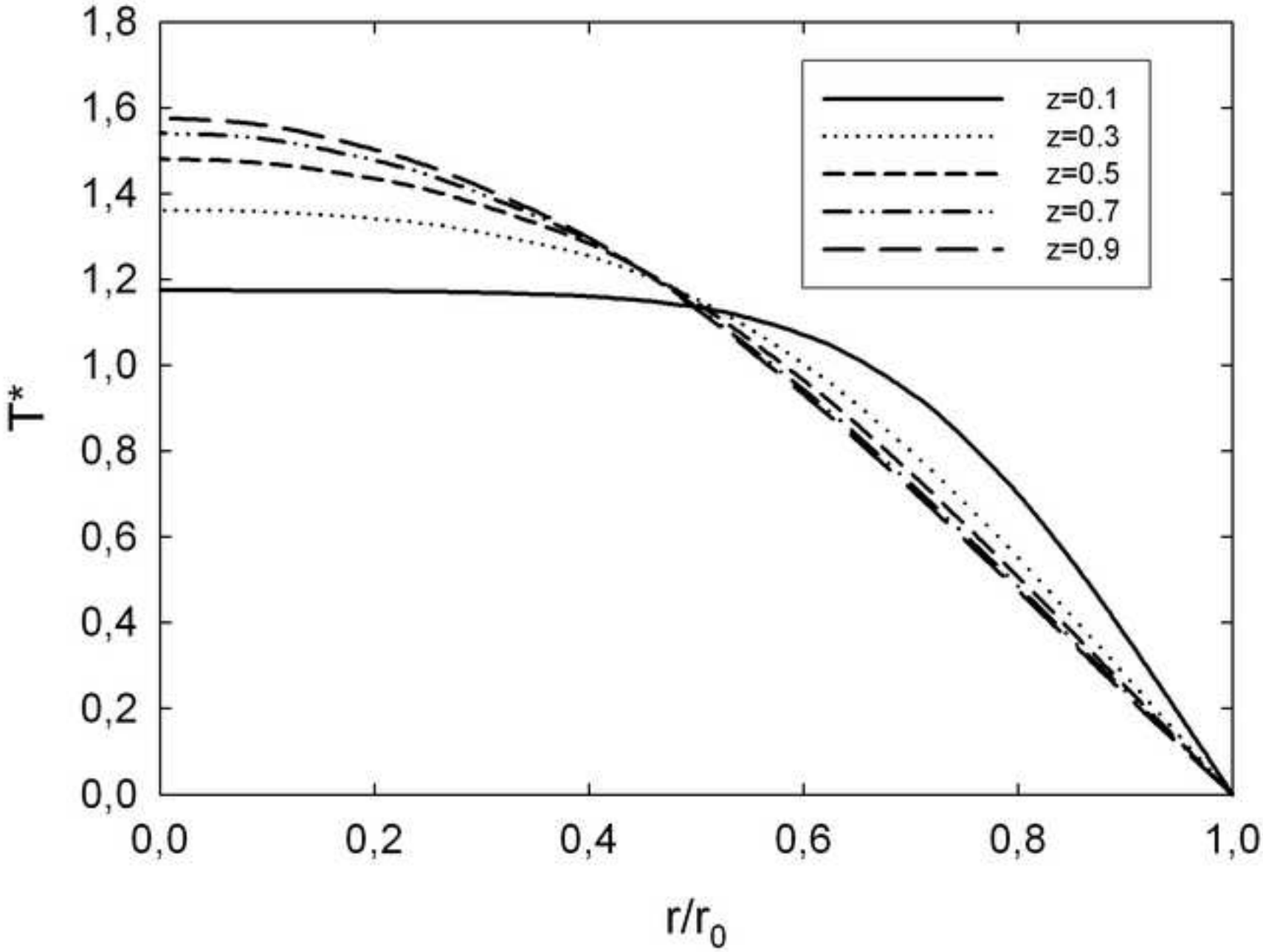
1,8
1,6
1,4
1,2
1,0
0,8
0,6
0,4
0,2
0,0
T*
0,0
0,2
0,4
0,6
0,8
1,0
r/r0
z=0.1
z=0.3
z=0.5
z=0.7
z=0.9

Figure 3b

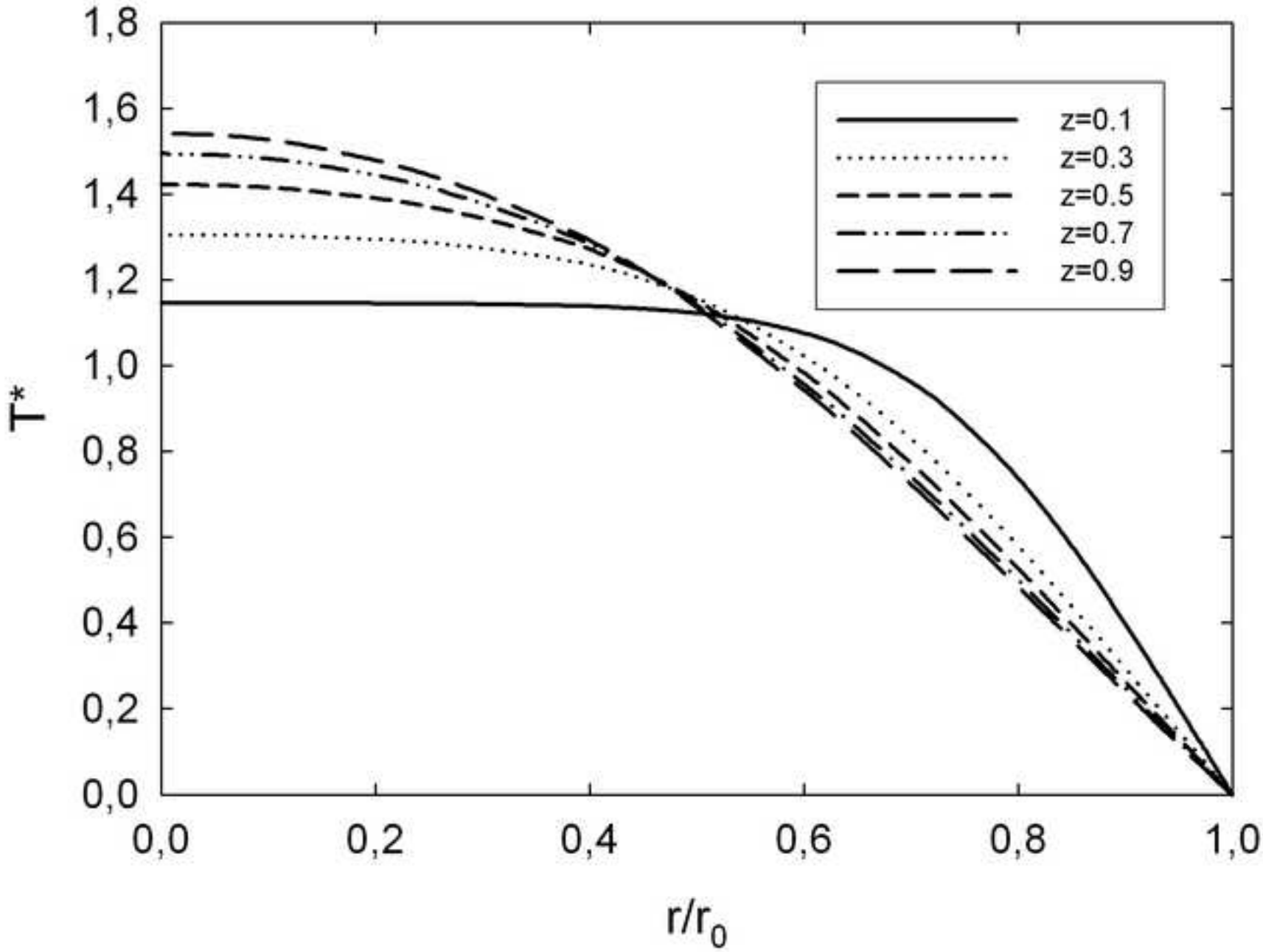
1,8
1,6
1,4
1,2
1,0
0,8
0,6
0,4
0,2
0,0
T*
0,0
0,2
0,4
0,6
0,8
1,0
r/r0
z=0.1
z=0.3
z=0.5
z=0.7
z=0.9

Figure 4a

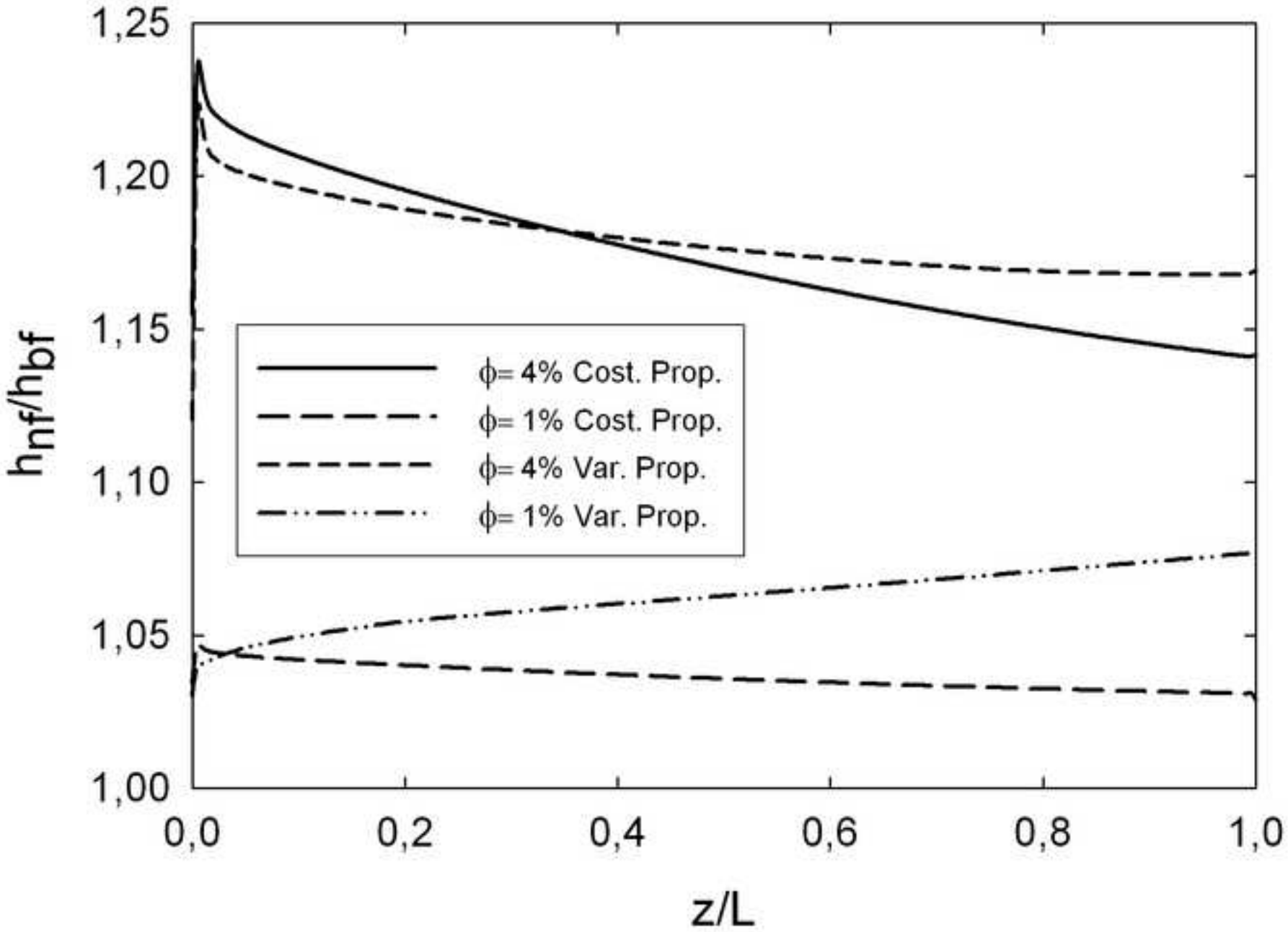
1,25
1,20
1,15
1,10
1,05
1,00
0,0
0,2
0,4
0,6
0,8
1,0
h_{nf}/h_{bf}
z/L
ϕ= 4% Cost. Prop.
ϕ= 1% Cost. Prop.
ϕ= 4% Var. Prop.
ϕ= 1% Var. Prop.

Figure 4b

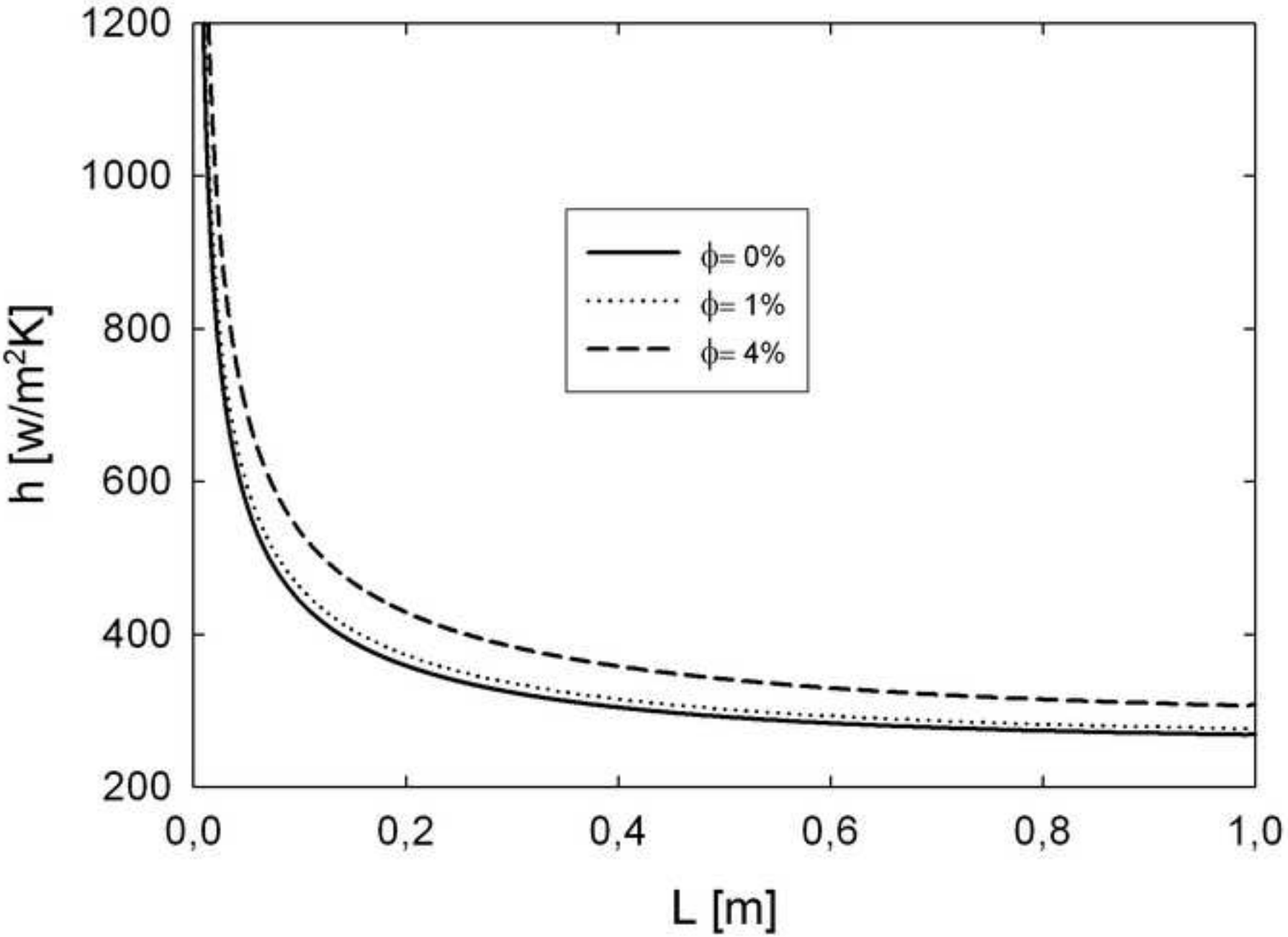

Figure 4c

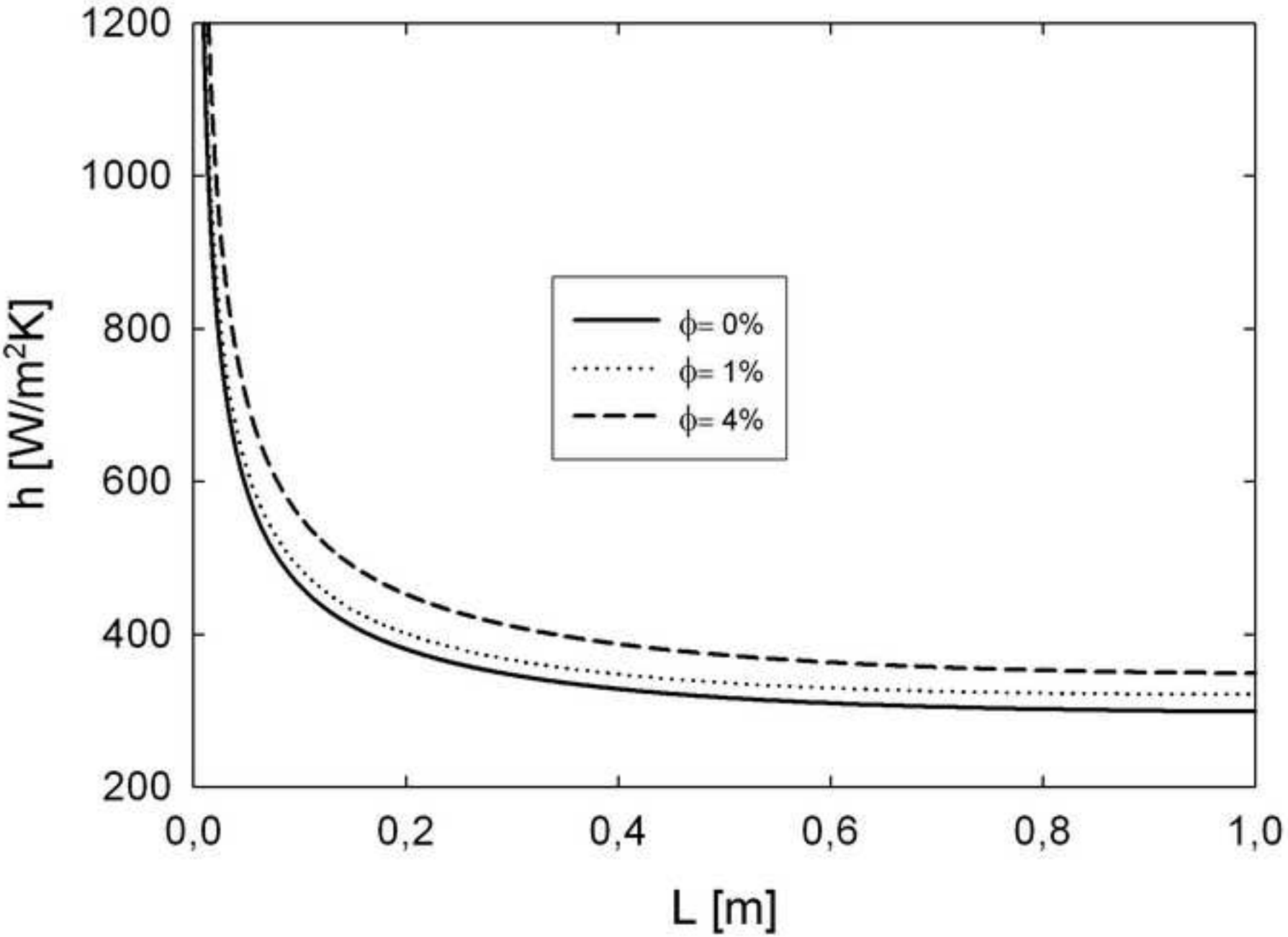

Figure 5a

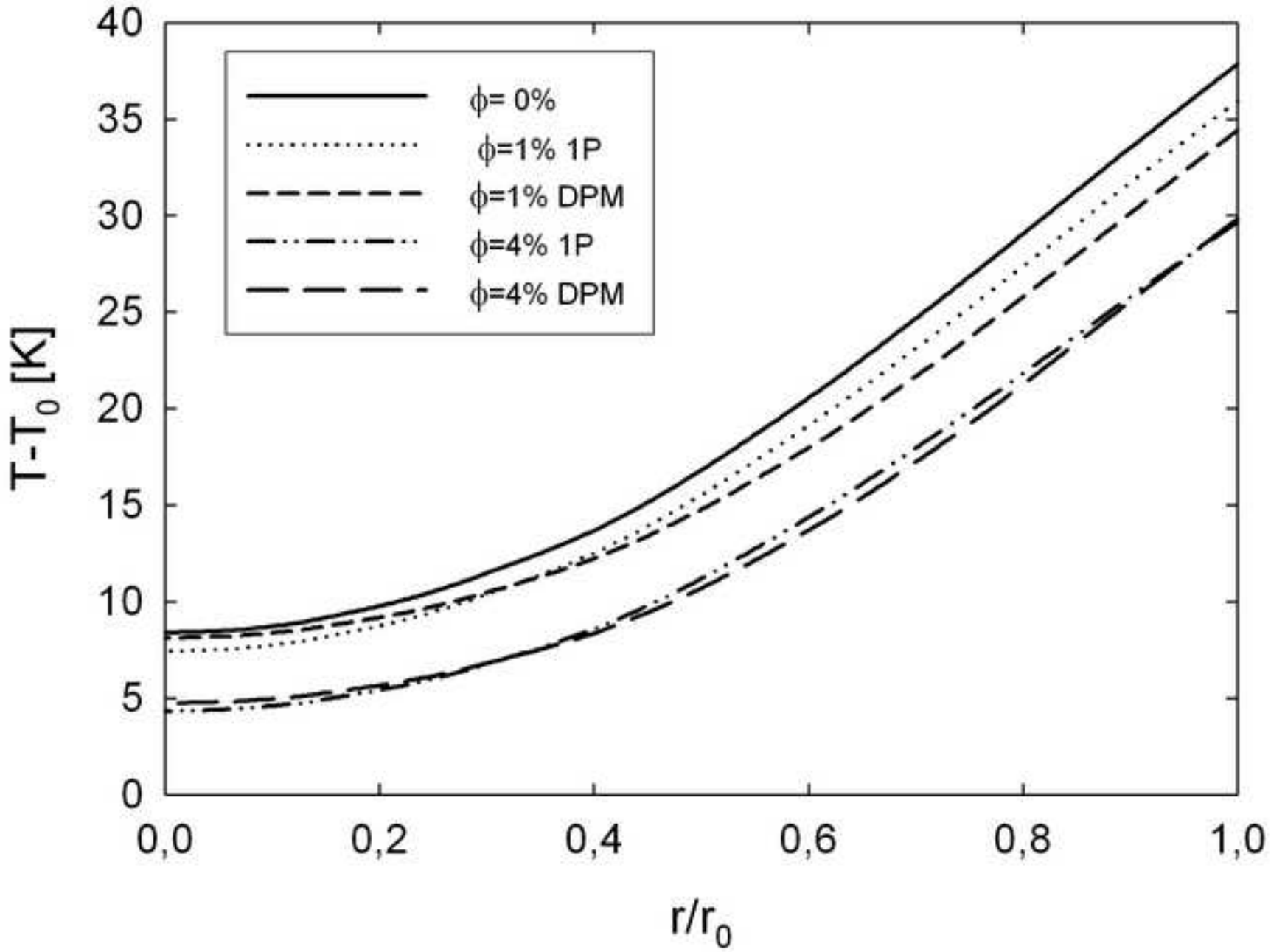
40
35
30
25
20
15
10
5
0
0,0
0,2
0,4
0,6
0,8
1,0
T-T0 [K]
r/r0
ϕ= 0%
ϕ=1% 1P
ϕ=1% DPM
ϕ=4% 1P
ϕ=4% DPM

Figure 5b

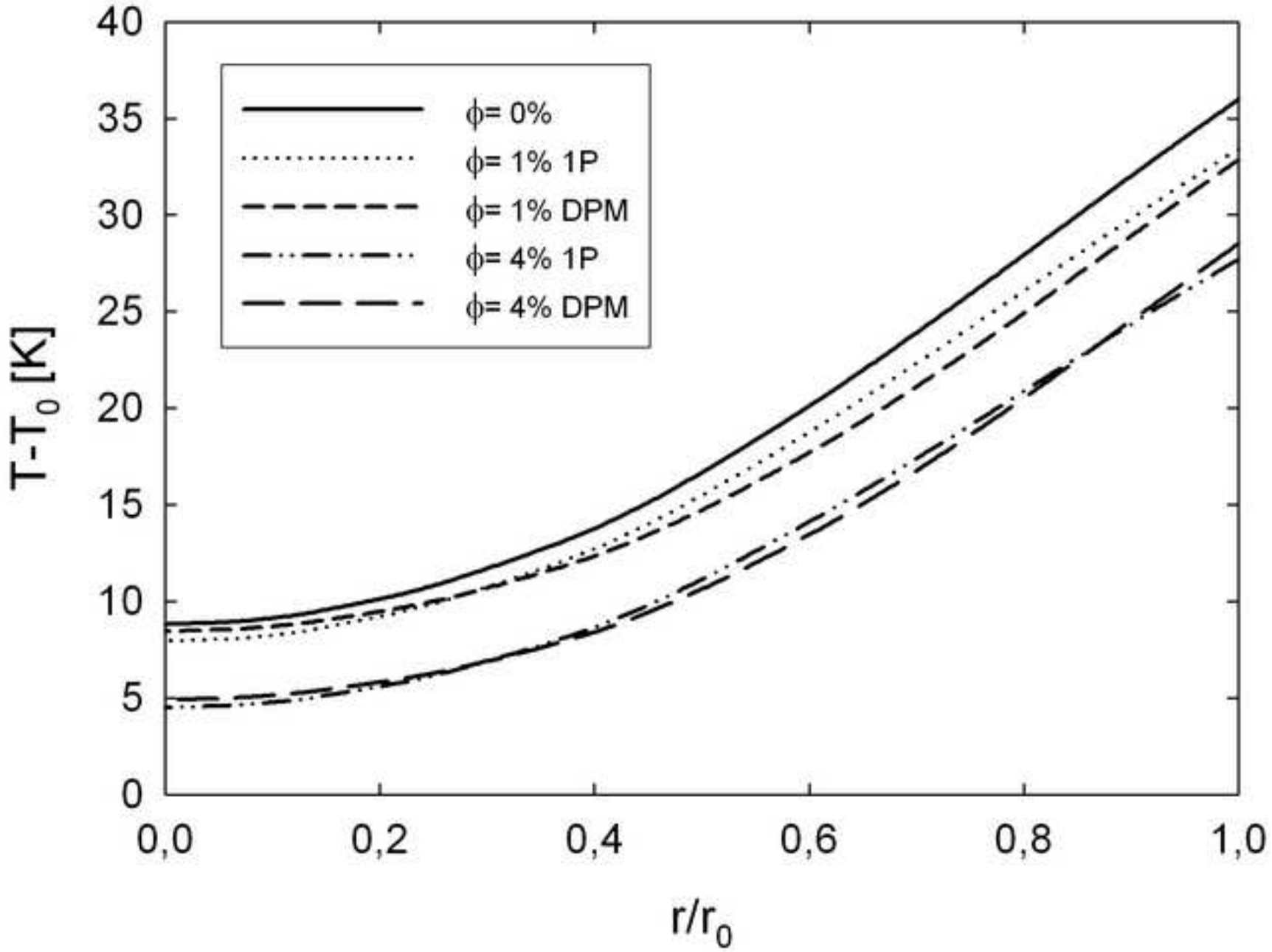
40
35
30
25
20
15
10
5
0
0,0
0,2
0,4
0,6
0,8
1,0
T-T0 [K]
r/r0
ϕ= 0%
ϕ= 1% 1P
ϕ= 1% DPM
ϕ= 4% 1P
ϕ= 4% DPM

Figure 6a

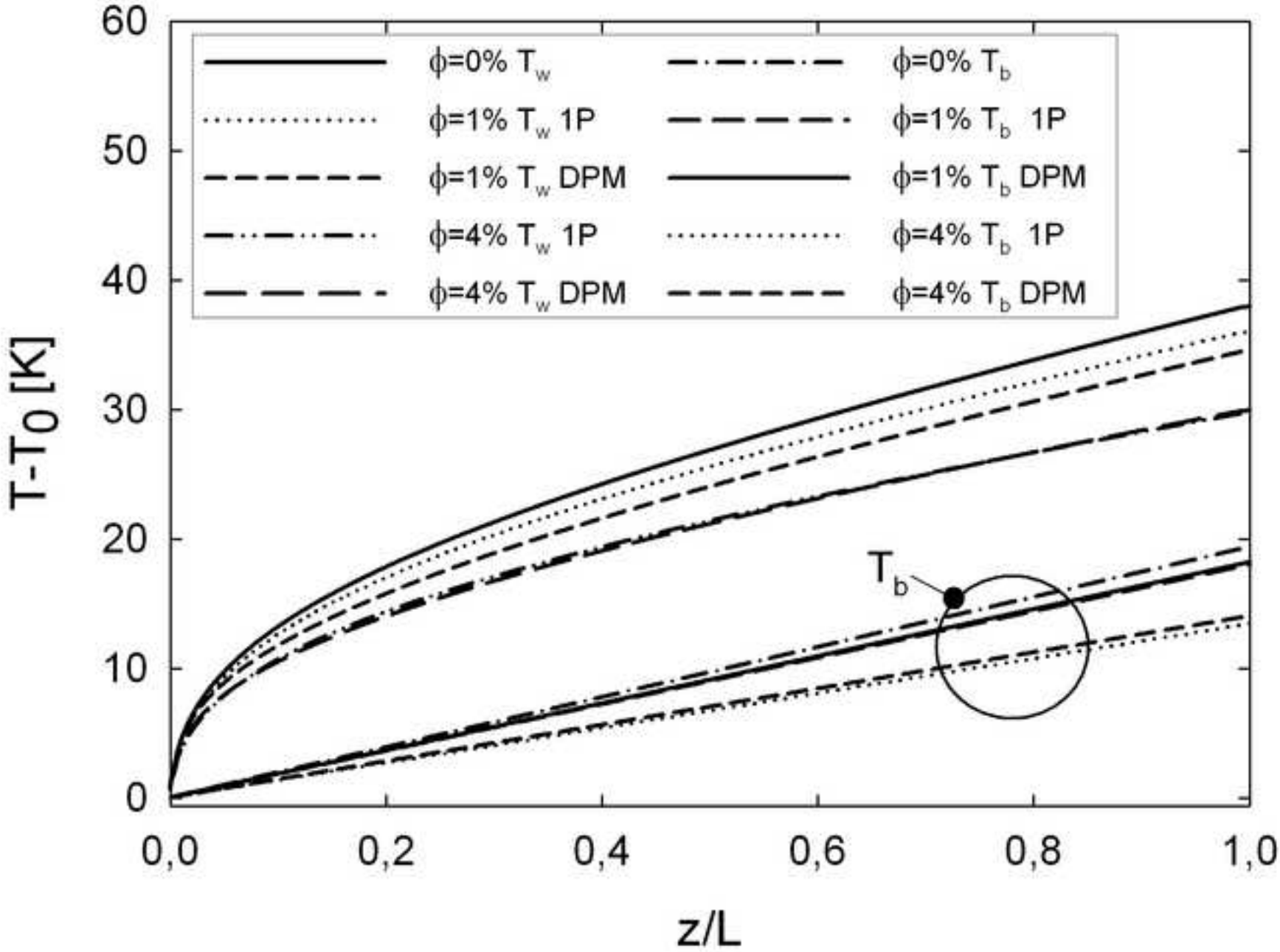
60
50
40
30
20
10
0
T-T0 [K]
0,0
0,2
0,4
0,6
0,8
1,0
z/L
ϕ=0% Tw
ϕ=0% Tb
ϕ=1% Tw 1P
ϕ=1% Tb 1P
ϕ=1% Tw DPM
ϕ=1% Tb DPM
ϕ=4% Tw 1P
ϕ=4% Tb 1P
ϕ=4% Tw DPM
ϕ=4% Tb DPM
Tb

Figure 6b

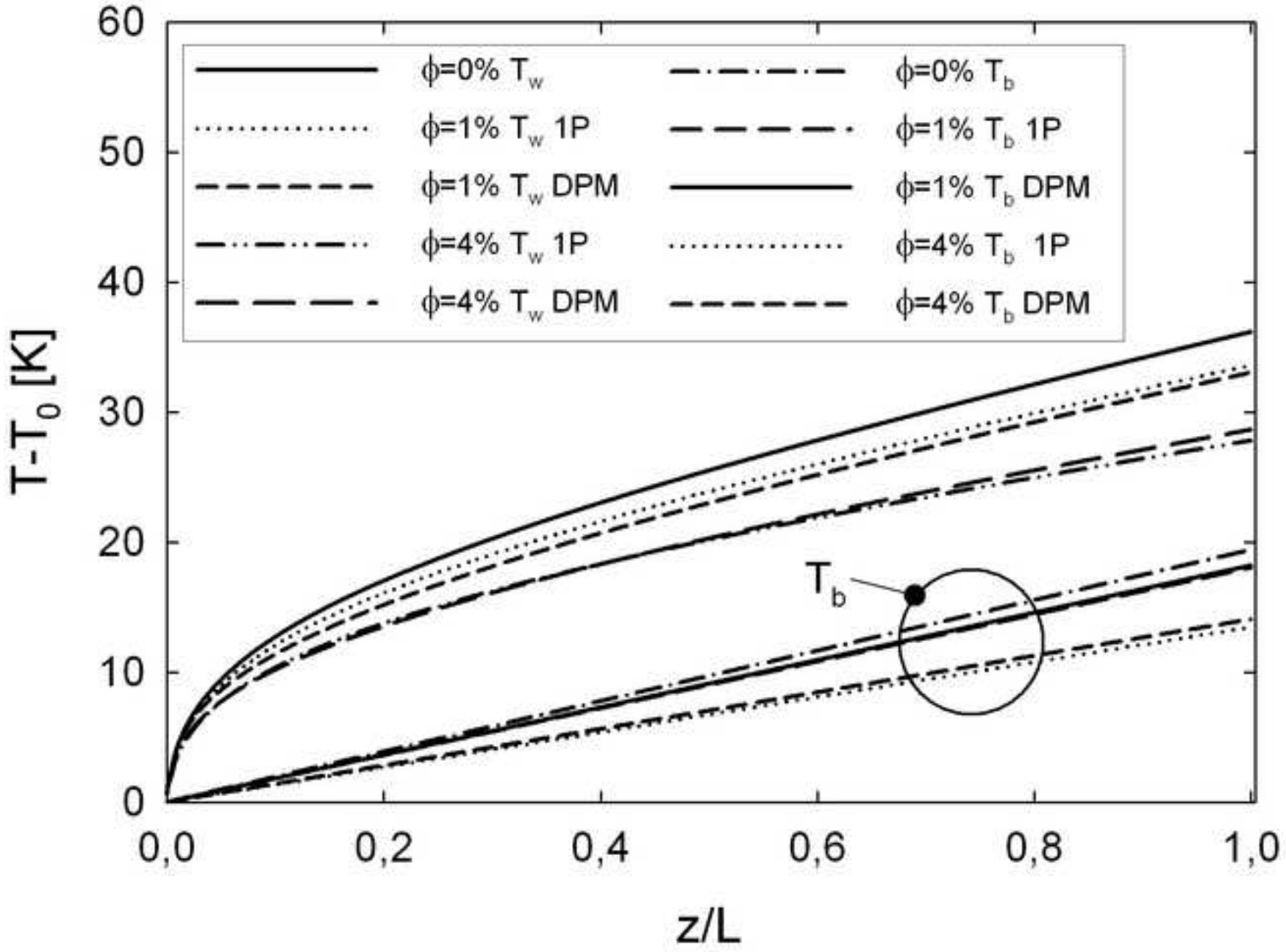
60
50
40
30
20
10
0
0,0
0,2
0,4
0,6
0,8
1,0
T-T0 [K]
z/L
ϕ=0% Tw
ϕ=0% Tb
ϕ=1% Tw 1P
ϕ=1% Tb 1P
ϕ=1% Tw DPM
ϕ=1% Tb DPM
ϕ=4% Tw 1P
ϕ=4% Tb 1P
ϕ=4% Tw DPM
ϕ=4% Tb DPM
Tb

Figure 7a

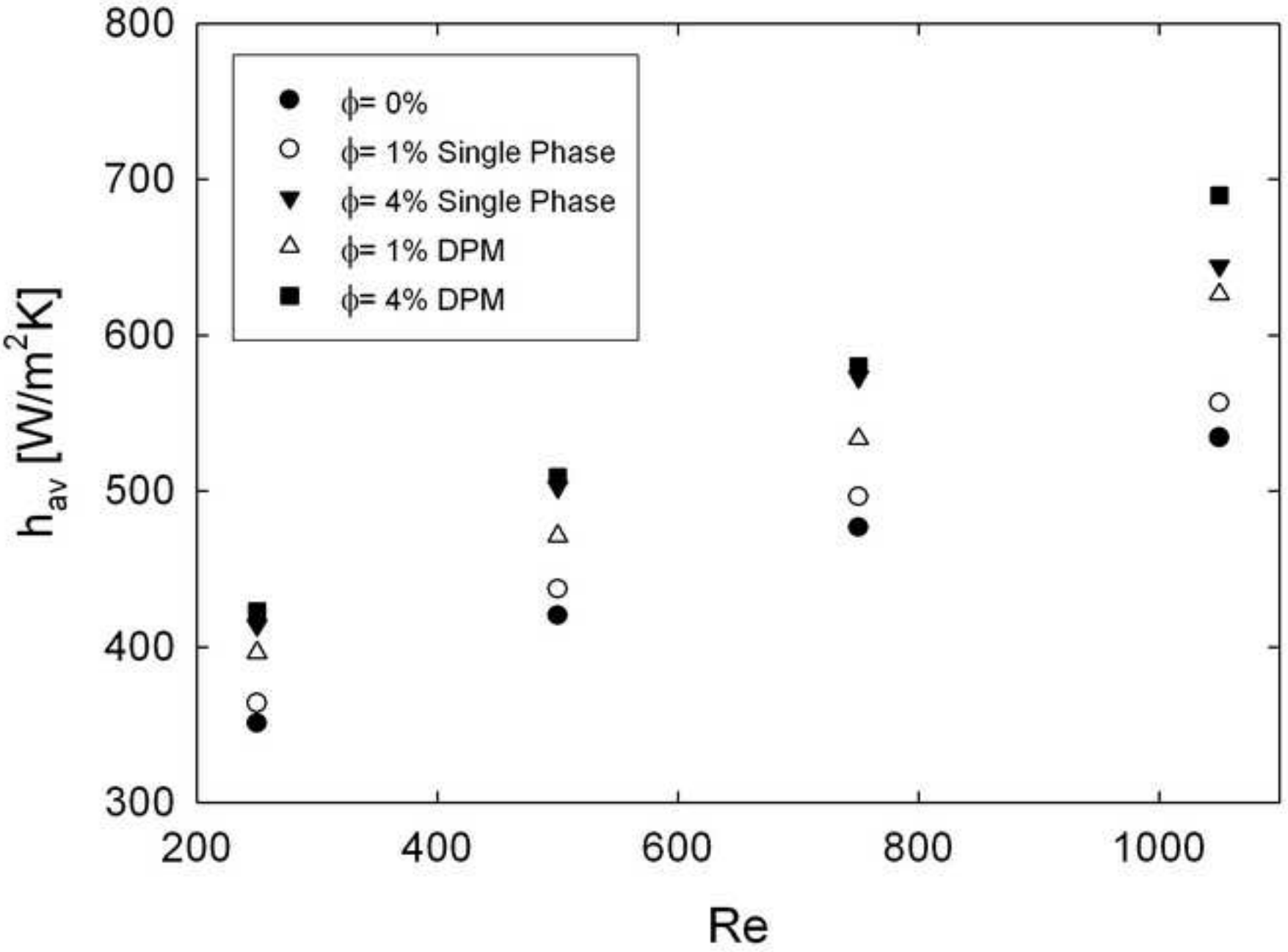
800
700
600
500
400
300
200
400
600
800
1000
Re
h_{av} [W/m^{2}K]
ϕ= 0%
ϕ= 1% Single Phase
ϕ= 4% Single Phase
ϕ= 1% DPM
ϕ= 4% DPM

Figure 7b

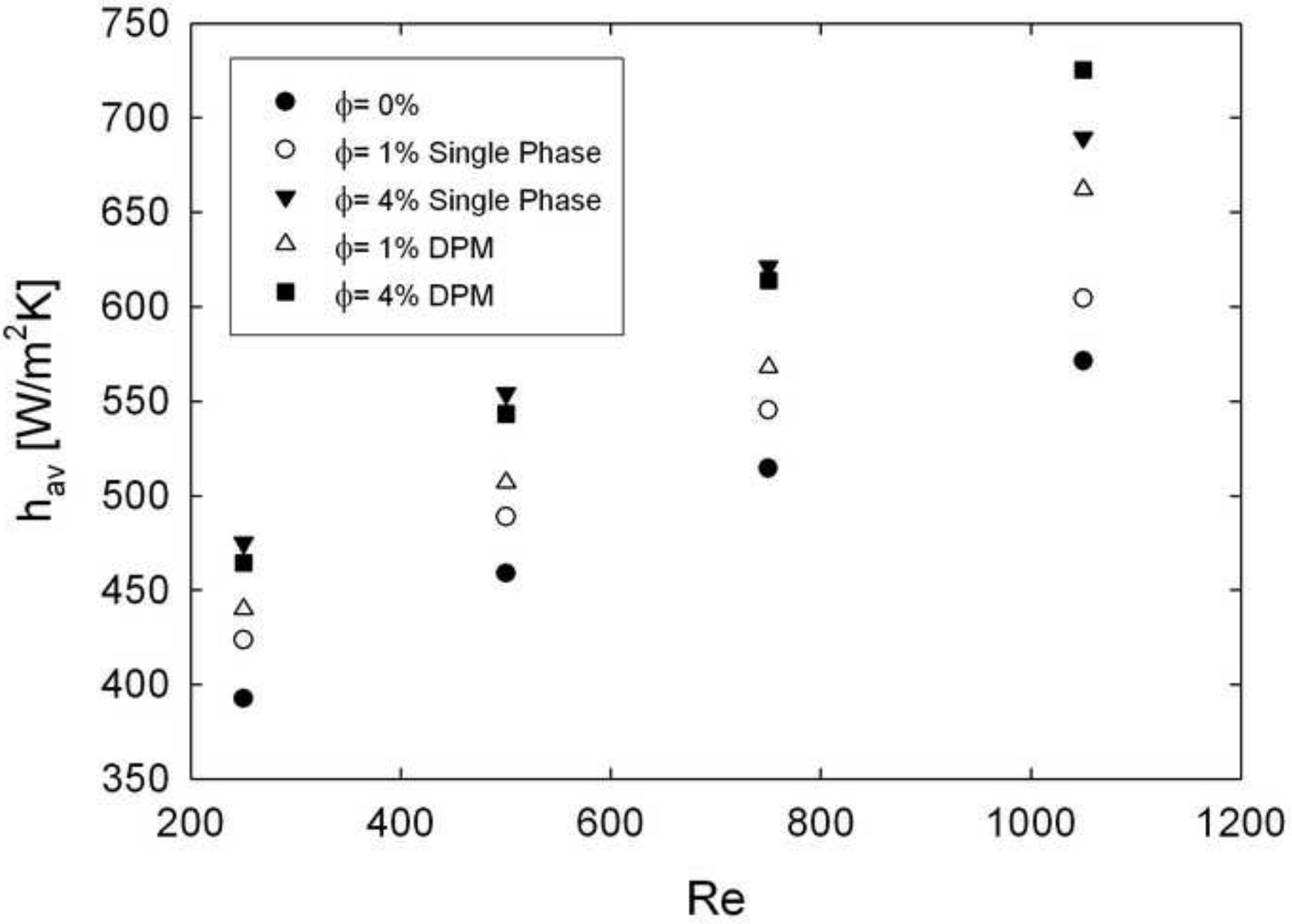
750
700
650
600
550
500
450
400
350
200
400
600
800
1000
1200
Re
h_{av} [W/m^{2}K]
ϕ= 0%
ϕ= 1% Single Phase
ϕ= 4% Single Phase
ϕ= 1% DPM
ϕ= 4% DPM

Figure 8a

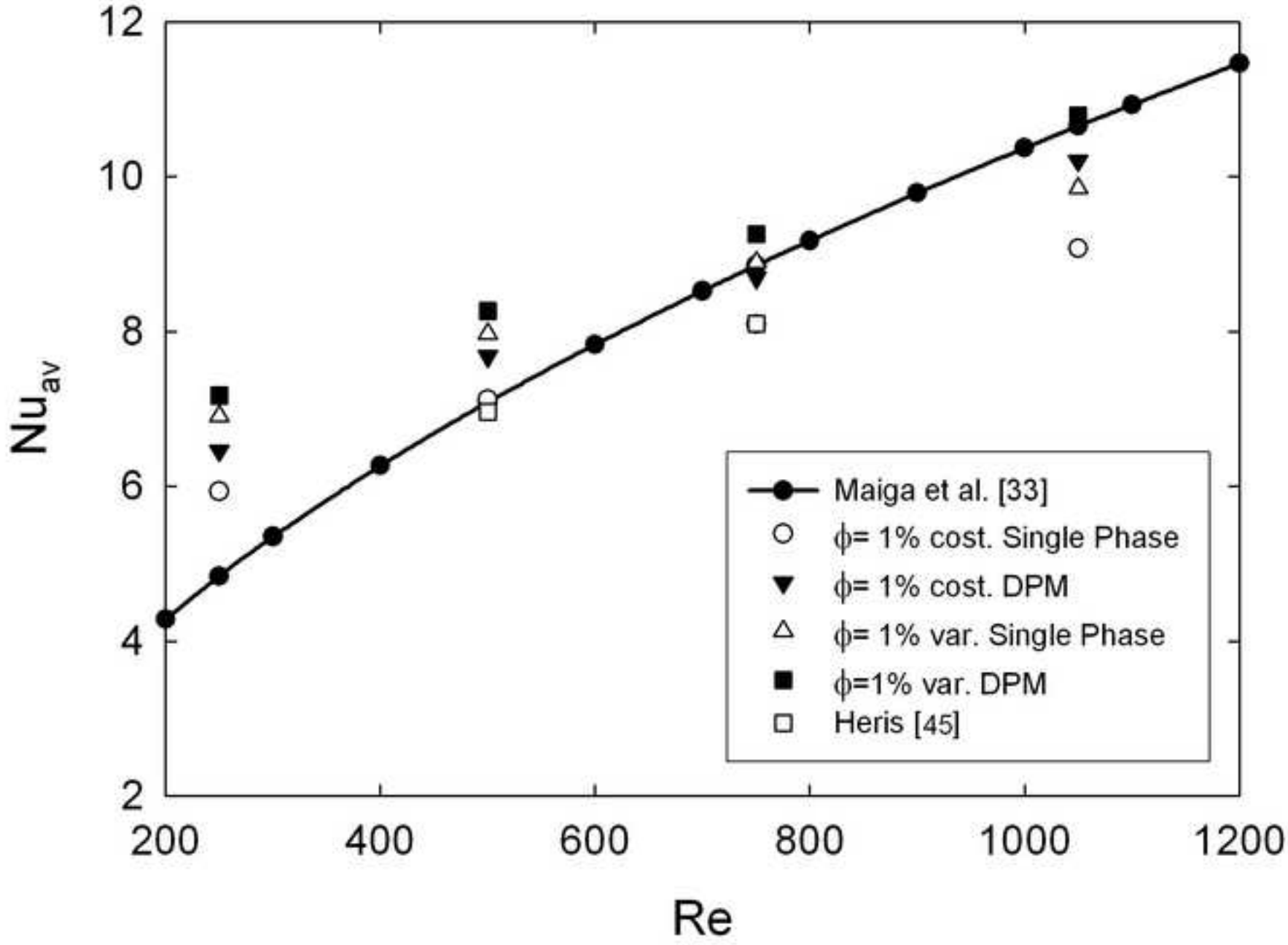
12
10
8
6
4
2
200
400
600
800
1000
1200
Nu_av
Re
Maiga et al. [33]
ϕ= 1% cost. Single Phase
ϕ= 1% cost. DPM
ϕ= 1% var. Single Phase
ϕ=1% var. DPM
Heris [45]

Figure 8b

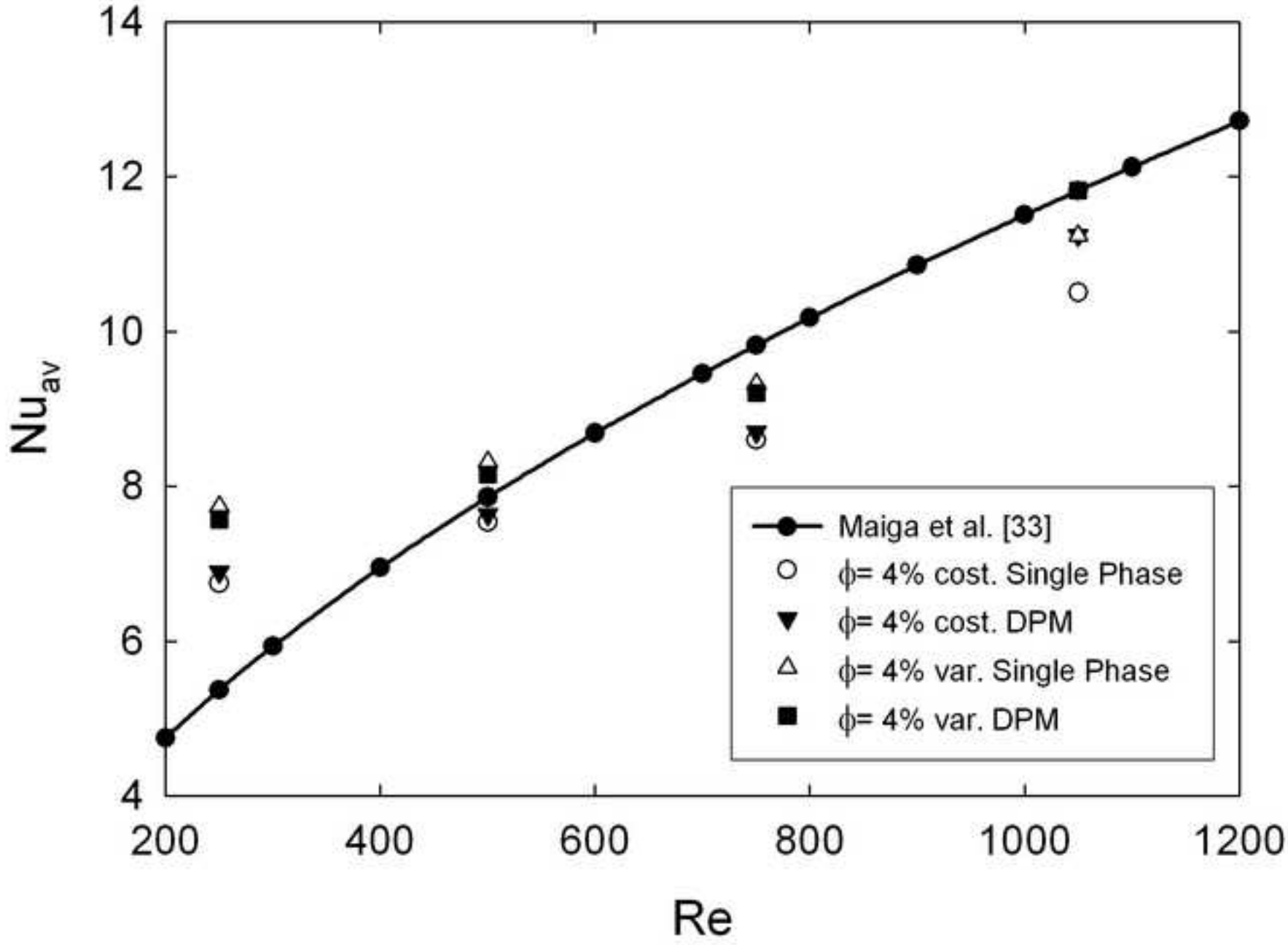
14
12
10
8
6
4
200
400
600
800
1000
1200
Nu_av
Re
Maiga et al. [33]
ϕ= 4% cost. Single Phase
ϕ= 4% cost. DPM
ϕ= 4% var. Single Phase
ϕ= 4% var. DPM

Table 1. Heat transfer coefficients for Re=250, q=5000W/m^2 and the investigated models.

Model		φ	h_{av} [W/m^{2}K]	h_{nf}/h_{bf}	Nu_{av}	Nu_{nf}/Nu_{bf}
H_2O	Cst.	0%	350.8	1	5.88	1
	Var.	0%	375.5	1	6.29	1
1-phase	Cst.	1%	363.9	1.037	5.93	1.009
	Var.	1%	397.7	1.059	6.48	1.030
2-phase	Cst.	1%	395.9	1.129	6.45	1.098
	Var.	1%	420.7	1.120	6.86	1.090
1-phase	Cst.	4%	413.8	1.180	6.75	1.148
	Var.	4%	443.6	1.181	7.23	1.150
2-phase	Cst.	4%	422.0	1.203	6.88	1.171
	Var.	4%	445.8	1.187	7.27	1.155

Table 2. Average and relative wall shear stress for Re=250, q=5000W/m^2 and the investigated models.

Model		φ	τ_{av} [Pa]	τ_{nf}/τ_{bf}
H_2O	Cst.	0%	0.0203	1
	Var.	0%	0.0145	1
1-phase	Cst.	1%	0.0232	1.145
	Var.	1%	0.0171	1.180
2-phase	Cst.	1%	0.0280	1.381
	Var.	1%	0.0206	1.419
1-phase	Cst.	4%	0.0403	1.987
	Var.	4%	0.0290	2.000
2-phase	Cst.	4%	0.0363	1.790
	Var.	4%	0.0278	1.920

Table 3. Values of h_{nf}/h_{bf} for Re=250, several heat fluxes and the investigated models.

	φ=1%				φ=4%			
	1-phase		2-phase		1-phase		2-phase	
q [W/m^2]	cst.	var.	cst.	var.	cst.	var.	cst.	var.
5000	1.037	1.059	1.129	1.120	1.180	1.181	1.203	1.187
7500	1.037	1.069	1.129	1.120	1.180	1.195	1.205	1.184
10000	1.037	1.079	1.130	1.120	1.180	1.209	1.205	1.183

Table 4. Values of τ_{nf}/τ_{bf} for Re=250, several heat fluxes and the investigated models.

	φ=1%				φ=4%			
	1-phase		2-phase		1-phase		2-phase	
q [W/m^2]	cst.	var.	cst.	var.	cst.	var.	cst.	var.
5000	1.145	1.180	1.380	1.419	1.987	2.000	1.790	1.920
7500	1.145	1.203	1.383	1.431	1.987	2.054	1.790	1.966
10000	1.145	1.234	1.380	1.447	1.987	2.135	1.791	2.012

Table 5. Comparison between numerical data from this work and experimental data from Wen and Ding [27].

	Wen & Ding [22]		1-phase				2-phase			
			Cst.		Var		Cst.		Var	
z/D	Nu	Nu_{nf}/Nu_{bf}	Nu	Nu_{nf}/Nu_{bf}	Nu	Nu_{nf}/Nu_{bf}	Nu	Nu_{nf}/Nu_{bf}	Nu	Nu_{nf}/Nu_{bf}
26	12.3	1.15	8.89	1.01	9.65	1.03	10.30	1.18	10.87	1.16
63	8	1.13	6.60	1.01	7.44	1.04	7.75	1.19	8.35	1.17